Master Thesis
平成13年度修士論文

Active Phenomena on the Solar Surface
— Essential Mechanism Producting such Phenomena —

太陽表面での活動現象
— 活動現象の発生メカニズム —

ASAI Ayumi
浅井 歩

DEPARTMENT OF ASTORONOMY, KYOTO UNIVERSITY
KWASAN AND HIDA OBSERVATORIES, KYOTO UNIVERSITY

February 1, 2002

Extended Abstract

Chapter 1. General Introduction

In this chapter, we review various active phenomena which occur on the solar surface, especially solar flares. We describe the relation among the phenomena based on the "unified model" suggested by Shibata et al. (1995).

Chapter 2. Fine Structures inside Flare Ribbons

We report a detailed examination of fine structures inside flare ribbons and the temporal evolution of such structure during an X2.3 solar flare which occurred on 2001 April 10. We observed the flare in Hα with the Sartorius Telescope at Kwasan Observatory, Kyoto University. Thanks to the short exposure time given for the flare, the fine structures were observed without saturating. First, we examined the temporal and spatial evolutions of the Hα kernels. We identified the conjugate foot points in each flare ribbon by calculating cross-correlation functions of the light curves of the Hα kernels. We found that those foot points are really connected with the flare loops seen in extreme-ultraviolet images obtained with the *Transition Region and Coronal Explorer*. The selected pairs of the Hα kernels show the various features in their sites and brightenings times. Investigating them, we have been able to follow the evolution of the energy release site during the flare. Second, we compared the spatial distributions of the hard X-ray (HXR) sources with those of Hα kernels. While many Hα kernels are found to brighten successively in the flare development, the HXR sources are locally confined in some special Hα kernels where the photospheric magnetic field shows the maximum strength. We estimated the energy release rates at each radiation source, and found that it is high enough at the HXR sources to make the difference of appearance.

Chapter 3. Quasi-Periodic Acceleration of Electrons

We present an examination of the multiwavelength observation of a

C7.9 flare that occurred on 1998 November 10. This is the first imaging observation of the quasi-periodic pulsations (QPPs). Four bursts were observed with the hard X-ray telescope aboard *Yohkoh* and the Nobeyama Radioheliograph during the impulsive phase of the flare. In the second burst, the hard X-ray and microwave time profiles clearly showed a QPP. We estimated the Alfvén transit time along the flare loop using the images of the soft X-ray telescope aboard *Yohkoh* and the photospheric magnetgrams and found that the transit time was almost equal to the period of the QPP. We therefore suggest, based on a shock acceleration model, that variations of macroscopic magnetic structures, such as oscillations of coronal loops, affect the efficiency of particle injection/acceleration.

Chapter 4. Plasma Ejections from a Light Bridge in a Sunspot Umbra

We present conspicuous activities of plasma ejections along a light bridge of a stable and mature sunspot in NOAA Active Region 8971 on 2000 May 2. We found the ejections both in the Hα (10^4 K) images obtained with the Domeless Solar Telescope at Hida Observatory and in the 171 Å (Fe IX/X; $\sim 10^6$ K) images obtained with the *Transition Region and Coronal Explorer*. Main characteristics of the ejections are as follows: (1) Ejections occur intermittently and recurrently. (2) The velocities and the timings of the 171 Å ejections are the same as those of Hα ejections. (3) The appearance of ejections are different from one another; i.e., the Hα ejections have jetlike appearance, while the 171 Å ejections are like loops.

Chapter 5. Future Directions

We summarize these topics and present future prospects.

Contents

List of Figures

List of Tables

Chapter 1

General Introduction

1.1 Active Phenomena

On the solar surface, we can see various kinds of active phenomena: flares, surges, coronal mass ejections (CMEs), and so on (see Figs. 1.1, 1.2, 1.3, respectively). In spite of the variety, release of magnetic energy is the essential mechanism that generates those phenomena in common.

Solar flares (Fig. 1.1 especially have been studied for a long time, since they are such prominent events among the active phenomena. Resent studies about solar flares have been developed with the ground based observations with very high spatial and temporal resolutions and satellite observations which have progressed rapidly in a few decades.

Solar flares are the response of the solar atmosphere to a sudden, transient release of energy (Bruzek & Durrant 1977). The temperatures attained in the chromosphere are $\approx 10^4$ K (chromospheric or low temperature flare; see the *left* panel of Fig. 1.1), in the corona $\approx 10^7$ K (high temperature flare; see the *right* panel of Fig. 1.1). The total energy release in the largest events is $\approx 10^{32}$ erg. Flares produce transient electromagnetic radiation over a vary wide range of wavelengths extending from hard X-rays ($\lambda \approx 10^{-9}$ em) - in very rare cases from γ-rays ($\lambda \approx 10^{-11}$ em) - to km radio waves (10^6 cm) (see Fig. 1.4).

Shibata et al. (1995) have suggested the "unified model" to explain the relation between solar flares and a lot of flare-associated phenomena, like plasma ejection, particle acceleration and so on, on the point of magnetic reconnection. Figure 1.5 show the cartoon of the unified model.

Solar flares, that is magnetic reconnection, leads both to a thermal plasma-heating and to an non-thermal plasma-acceleration (Bruzek & Durrant 1977). Therefore, both the thermal and non-thermal processes have been an impor-
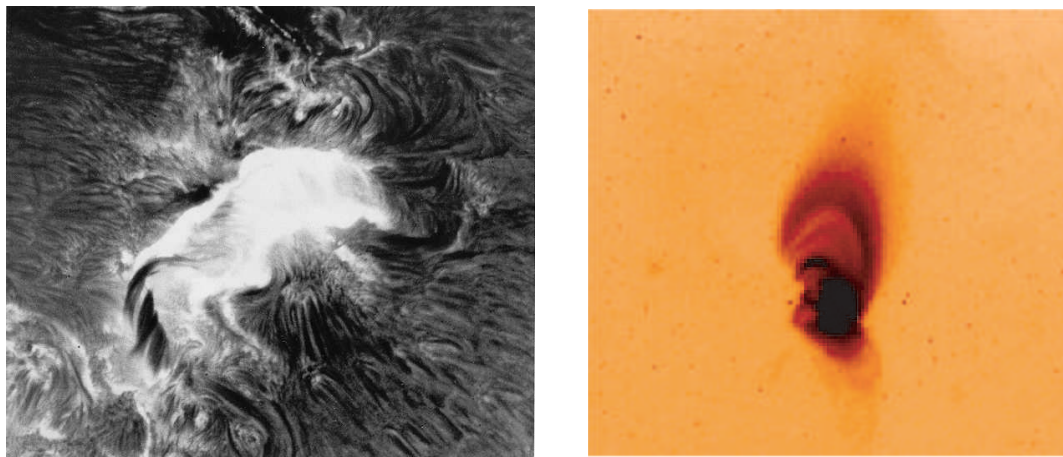
Figure 1.1: An example of a solar flare. *Left*: Hα image taken with Dome-less Solar Telescope at Hida Observatory. *Right*: Coronal image taken with *Yohkoh*/SXT.

tant topic in studying solar flares.

1.1.1 Particle Acceleration

The magnetic reconnection leads to the non-thermal acceleration of particles. The number of accelerated electrons is about 10^{33-35} electrons s^{-1}, and the electrons are accelerated up to ≈ 10 MeV, and ions are up to ≈ 1 GeV (e.g., Aschwanden 2002). These energetic particles radiate hard X-rays (HXRs), γ-rays, and microwaves. The observed photon count rates are fitted approximately with power-law functions $I(E) \propto E^{-\gamma}$, where γ is the spectral index of photon and range from 2 to 7. The spectral of the accelerated electrons also show power law distributions $N_e(E) \propto E^{-\delta}$, where δ is the spectral index of electron and range from 3 to 6.

The mechanism of the particle acceleration is basic in the physics and important to study various phenomena. Although various models to explain those observational features have been suggested until now, the mechanism is so difficult and still remained as an unsolved problem. We can only investigate the global structure of energy release by using beautiful images obtained with various instruments. We need to challenge to solve the problem on such a point of the "solar physics".
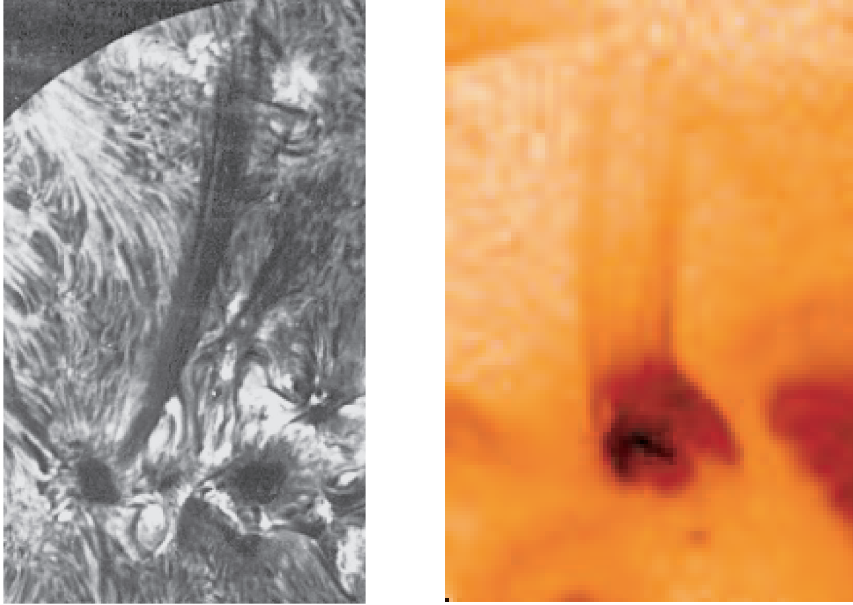
Figure 1.2: An example of plasma ejections. *Left*: Hα surge taken with DST at Hida Observatory. *Right*: X-ray jet taken with *Yohkoh*/SXT. (Shimojo et al. 1996)

1.1.2 Plasma Ejection

The magnetic reconnection also leads to thermal heating of plasma. These are seen in Hα as Hα surges (e.g., Roy 1973) and filament eruptions, and in X-rays as X-ray jets (e.g., Shimojo 1996) on the solar surface, and ejected plasmoids on the limb. The mechanism of the thermal plasma-heating among Hα surges, X-ray jets, CMEs, and so on is considered to be common, although the scale of the events is various again.

solar jets

Both Hα surges (the *left* panel in Fig. 1.2) and X-ray jets (the *right* panel in Fig. 1.2) are plasma ejections whose trajectories show clearly collimated structure (jet-like structure). Many studies about Hα have been done for a long time (e.g., Roy 1973). Hα surges show the ejections of the plasma whose temperature is $\sim 10^4$ K which are caused by magnetic reconnection in the chromosphere. On the other hand, the studies about X-ray jets have been promoted with the soft X-ray telescope (Tsuneta et al. 1991) aboard *Yohkoh* (Ogawara et al. 1991) and analyzed in detail by Shimojo et al. (1996). The average temperature is much higher, and $\sim 5 \times 10^6$ K, which are caused by the magnetic
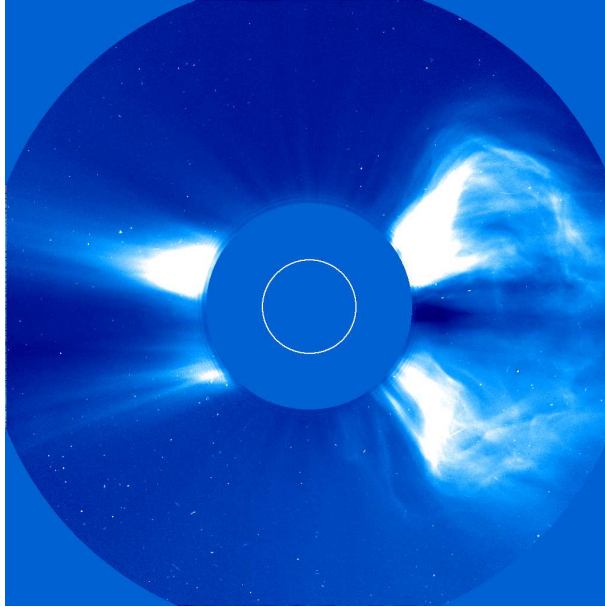
Figure 1.3: An example of a CME taken with *SOHO*/LASCO.

reconnection in the solar corona. The collimated structure indicates the confinement with the surrounding magnetic field.

Kurokawa (1988) and Kurokawa & Kawai (1993) have reported that Hα surges are often found at the earliest stage of emerging flux regions (EFRs). X-ray jets are often found in EFRs, too (Shibata et al. 1992; Shimojo et al. 1996). Magnetic reconnection between a newly emerging flux and a pre-existing magnetic field is the essential mechanism of production of Hα surges and X-ray jets (Kurokawa & Sano 2000), though the size of such EFR-associated surges is smaller than that of typical flare-associated surges. Moreover, Yokoyama & Shibata (1995) showed in their numerical simulation that such a reconnection really produces Hα surges in EFRs.

CMEs and filament eruptions

Large flares are sometimes associated with huge mass ejections. Figure 1.3 shows an exampe of CME. They show balloon-like shape and they expand as rising above the solar corona. CME releases mass of up to 10^{14} g, and the speed reaches up to 10^8 cm s^{-1}.

Filament eruptions which are seen in Hα also associate with large flares. Filaments are high-density and low-temperature plasma which are floated in the corona and supported with coronal magnetic field.

Profile of Solar Flare

Microwave

Hα line

Soft X-ray

Hard X-ray

Impulsive

Main

Precursor

Relative Radiation Flux

TIME [min]
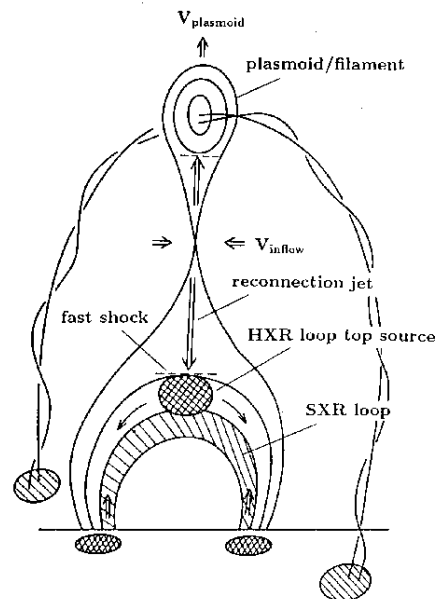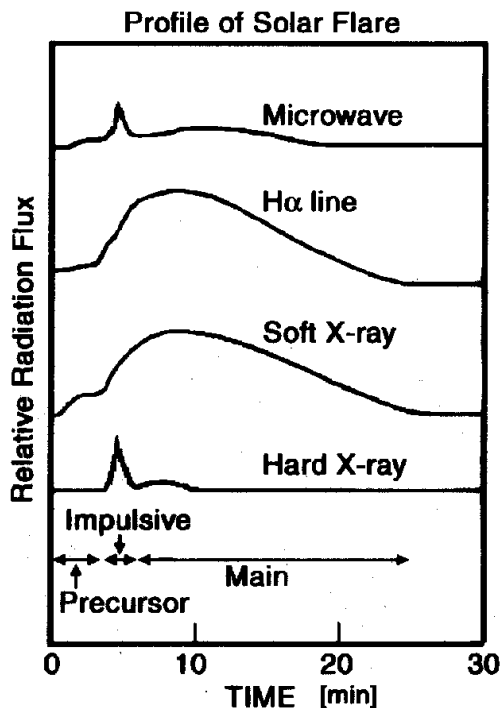
Figure 1.4: Time profiles of solar flares. (based on Kane 1974)

Figure 1.5: Unified model of magnetic reconnection. (Shibata et al. 1995)

When large flares occur they are erupted explosively. Filaments are thought to become the cores of CMEs, and filament eruptions and CMEs are thought to be exactly the same phenomena (see Fig. 1.5).

1.2   Aim of This Thesis

In this thesis we aim to solve the energy release mechanisms of active phenomena. We present a detailed examinations of various active phenomena which are observed on the solar surface, and discuss the relations of those phenomena with magnetic field structures.

We mainly used Hα data with high temporal and spatial resolutions obtained at Kwasan and Hida observatories, Kyoto University. We also used data obtained with another ground based observatory, Nobeyama Radio Observatory, and some satellites: *Yohkoh, SOHO*[1] ;Scherrer et al. 1995), and

---

[1]Solar & Heliospheric Observatory

TRACE[2] ;Handy et al. 1999; Schrijver et al. 1999).

Chapter 2

Using Hα data of the 2001 April 10 solar flare, we examine in detail the fine structure inside the flare ribbons, and the temporal evolution of such structure. We also follow the whole history of energy release in the flare. Then we examine the relation between the evolution of the flare ribbons and the amount of released energy.

Chapter 3

Non-thermal particles that are generated at the beginning phase of a solar flare are mainly observed in microwaves and HXR. The short-lived non-thermal bursts, which appear in those wavelengths, often show quasi-periodical natures. We examine the relation between the clear periodic pulsation, which was observed in the solar flare on 1998 November 10, and the global and macroscopic magnetic configuration. We also discuss the affect of the macroscopic configuration of the magnetic structure on the efficiency of acceleration of nonthermal particles.

Chapter 4

We examine the mechanism of plasma ejections from a light bridge observed on 2000 May 2. Light bridges sometimes locate in the middle of sunspot umbrae where magnetic field is high and active phenomena are thought to be restricted. The observed surge activities from the light bridge, however, indicate a possibility of emergence of magnetic fluxes there.

Chapter 5

We present future works and perspectives.

---

[2]Transition Region And Coronal Explorer

Bibliography

Aschwanden M. J., 2002, Space Sci. Rev., in press

Bruzek, A., and Durrant, C. J., 1977, Astrophysics and Space Science Library, 69, Illustrated Glossary for Solar and Solar-Terrestrial Physics, (Dordrecht: Reidel)

Handy, B. N., et al., 1999, Solar phys., 187, 229

Kane, S. R., 1974, Impulsive (flash) phase of solar flares: hard X-ray, microwave, EUV, and optical observations, in *Coronal disturbances* (ed. G. Newkirk), Proc. 54th IAU Symp., Reidel, Dordrecht, p. 105

Kurokawa, H., 1988, VA, 31, 67

Kurokawa, H., & Kawai, G., 1993, in ASP Conf. Ser., 46, The Magnetic and Velocity Fields of Solar Active Regions, ed. H. Zirin, G. Ai, & H. Wang (San Francisco: ASP), 507

Kurokawa, H., & Sano, S., 2000, Adv. Space Res., 26, 441

Ogawara, Y., Takano, T., Kato, T., Kosugi, T., Tsuneta, S., Watanabe, T., Kondo, I., & Uchida, Y., 1991, Solar phys., 136, 10

Scherrer, P. H., et al., 1995, Solar phys., 162, 129

Schrijver, C. J., et al., 1999, Solar phys., 187, 261

Shibata, K., Ishido, Y., Acton, L. W., Strong, K. T., Hirayama, T., Uchida, Y., Mcallister, A. H., Matsumoto, R., Tsuneta, S., Shimizu, T., Hara, H., Sakurai, T., Ichimoto, K., Nishino, Y., Ogawara, Y., 1992, Publ. Astron. Soc. Japan, 44, L173

Shibata, K., Masuda, S., Shimojo, M., Hara, H., Yokoyama, T., Tsuneta, S., Kosugi, T., Ogawara, Y., 1995, Astrophys. J., 451, L83

Shimojo, M., Hashimoto, S., Shibata, K., Hirayama, T., Hudson, H. S. and
    Acton, L. W., 1996, Publ. Astron. Soc. Japan, 48, 123

Tsuneta, S., et al., 1991, Solar phys., 136, 37

Yokoyama, T., & Shibata, K., 1995, Nature, 375, 42

Chapter 2

Fine Structure inside Flare Ribbons and the Temporal Evolution of such Structure

We report a detailed examination of fine structures inside flare ribbons and the temporal evolution of such structure during an X2.3 solar flare which occurred on 2001 April 10. We observed the flare in Hα with the Sartorius Telescope at Kwasan Observatory, Kyoto University. Thanks to the short exposure time given for the flare, the fine structures were observed without saturating. First, we examined the temporal and spatial evolutions of the Hα kernels. We identified the conjugate foot points in each flare ribbon by calculating cross-correlation functions of the light curves of the Hα kernels. We found that those foot points are really connected with the flare loops seen in extreme-ultraviolet images obtained with the *Transition Region and Coronal Explorer*. The selected pairs of the Hα kernels show the various features in their sites and brightenings times. Investigating them, we have been able to follow the evolution of the energy release site during the flare. Second, we compared the spatial distributions of the hard X-ray (HXR) sources with those of Hα kernels. While many Hα kernels are found to brighten successively in the flare development, the HXR sources are locally confined in some special Hα kernels where the photospheric magnetic field shows the maximum strength. We estimated the energy release rates at each radiation source, and found that it is high enough at the HXR sources to make the difference of appearance.

9

2.1   Introduction

Non-thermal particles generated in the impulsive phase of solar flares are mainly observed in microwaves, hard X-rays (HXRs), and γ-rays. Observations in Hα also give important informations about the precipitations of nonthermal particles into the chromosphere with a higher spatial resolution than in other wavelengths (Kurokawa, Takakura, & Ohki 1988).

Non-thermal particles are considered to be accelerated near the energy release site, and to flow with very high speed along the flare loops. The speed is as high as about one-third of the speed of light ($\sim 10^5$ km s^{-1}). Therefore, they bombard the chromospheric plasma at both the foot points of the flare loops almost simultaneously. This happens even when an energy release site does not locate exactly on the loop top and an asymmetry energy release occurs, because of such high speed of non-thermal particles. The temporal evolutions of the intensities of both the foot points are very similar (Kurokawa *et al.* 1988; Sakao 1994). Although the mechanism of the particle acceleration remains unresolved, the location and time of the acceleration and/or of the energy release can be determined, if we precisely find the highly-correlated pairs of foot points and the times of precipitations.

First, in this paper, we precisely determine the location and the time of the precipitations using Hα data of the 10 April 2001 flare, and examine the evolution of the energy release sites. Location and light curve of HXR sources show high correlations with those of Hα kernels, because the bombardments stimulate the excitations and ionizations of hydrogen atoms which cause the enhanced Hα emissions in a short time (Kurokawa *et al.* 1988; Trottet *et al.* 2000; Wang *et al.* 2000; Qiu *et al.* 2001). Moreover, flare observations with higher spatial resolution are achieved by using Hα images than by HXRs and microwaves. We can investigate the precipitation sites of the particles with higher spatial resolution using Hα images (Kitahara & Kurokawa 1990). On the other hand, it has been not so easy to judge whether highly-correlated pairs of Hα kernels are really connected with flare loops. For example, although Kurokawa et al. (1992) examined relation of spatial configuration between Hα bright kernels and flare loops using soft X-ray (SXR) images obtained with the soft X-ray telescope (SXT; Tsuneta et al. 1991) aboard *Yohkoh* (Ogawara et al. 1991), they could not precisely confirm because the spatial resolution of the SXT was not high enough for discrete flare loops to be distinguished. Recently, spatial resolution to observe flare loops has been much improved by the extreme-ultraviolet (EUV) images obtained with the *Transition Region and Coronal Explorer* (*TRACE*; Handy et al. 1999). The images give us the informations about post-flare loops with much higher resolution than before. Therefore, we examine whether the highly-correlated

pairs are really connected with flare loops by using the *TRACE* 171 Å data.

Second, we compare the locations and timings of the HXR sources with those of Hα kernels, and discuss the energy release at the HXR sources. HXR images obtained with the hard X-ray telescope (HXT; Kosugi *et al.* 1991) aboard *Yohkoh* often show only a few HXR sources, except the HXR flare ribbons in the Bastille Day event on 14 July 2000 (Masuda 2001, private communications). HXR sources are accompanied with Hα kernels in many cases, but many Hα kernels are not accompanied with HXR sources. Such difference of spatial distributions between Hα and HXR sources is explained by the difference of the amount of released energy at each source and the low dynamic range of HXT. The energy release rate in solar flares is considered to depend on magnetic field strength and inflow velocity into reconnection region. To check the idea, we measured the photospheric magnetic field strength at each source and investigated its relation with the amount of released energy. Moreover, we examined relation of the timing of HXR brightenings with the separation speed of Hα flare ribbons. We then discuss the factors that affects the amount of released energy.

In §2.2 we summarize the observational data. In §2.3 we determine the conjugate foot points of Hα kernels, and examine the spatial and temporal evolutions of the Hα kernels and the energy release sites. In §2.4 we examine the relation between the energy release and the evolution of the flare ribbons. In §2.5 the summary and the discussion are given.

2.2   Observations

We have observed a big two-ribbon flare (X2.3 on the GOES scale) which occurred in the NOAA Active Region 9415 (S22°, W01°) at 05:10 UT, 2001 April 10 with the Sartorius 18cm Refractor Telescope (*Sartorius*) at Kwasan Observatory, Kyoto University. The Hα monochromatic images of the flare were obtained with the the Halle Lyot filter in Hα line center of 0.5 Å bandwidth and the Kodak Megaplus CCD Camera in The temporal and spatial resolution of the *Sartorius* data are about 2 s and $1''$, respectively. The left panels of Figure 2.2 (I to V) are the *Sartorius* images which show temporal evolutions of Hα flare ribbons. Thanks to the short exposure time given for the flare, the Hα images clearly show the fine structures inside the flare ribbons. The Hα kernels which successively appeared during the impulsive phase were clearly observed without saturating. Therefore, we can precisely study the temporal variations of the foot points precipitated by nonthermal electrons.

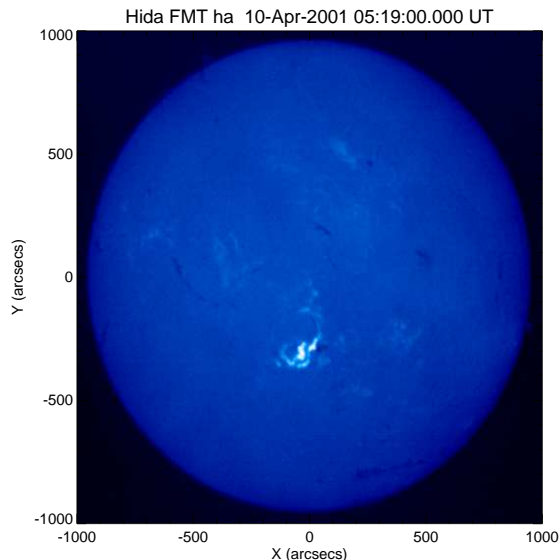The EUV images of the flare were obtained with *TRACE*. The pixel size

Figure 2.1: Hα full disk image of the flare at 05:19 UT taken with Flare Monitoring Telescope at Hida Observatory, Kyoto University. Solar north is up, and west is to the right.

of the *TRACE* CCD corresponds to $0''.5$ on the sun. *TRACE* 171 Å images clearly show the post-flare loops which confine 1 MK-plasma. The right panels of Figure 2.2 (VI to X) show the temporal evolutions of the flare ribbons and the flare loops seen in the *TRACE* 171 Å images. The flare ribbons in the *TRACE* 171 Å images appear almost simultaneously with Hα flare ribbons, or just after the energy release as the result of the precipitation of nonthermal particles. On the other hand, the formation of the 171 Å post-flare loops are found after the evolution of the flare ribbons. This is because it takes a certain time for hot plasma, which are heated up to about 10 MK or more to cool down to 1 MK. In the formation of the 171 Å post-flare loops, we notice the successive changes of loop structure: tightly sheared loops are observed at the beginning, and more relaxed loops at the later stage. Here, the word "sheared" means that flare loops lie parallel to the neutral line, and "relaxed" means that they lie perpendicularly to the neutral line.

To examine nonthermal particles, we used the microwave total flux measured with Nobeyama Radioheliograph (NoRH; Nakajima et al. 1994), and the HXR data obtained with *Yohkoh*/HXT. These have temporal resolutions of 0.1 s and 0.5 s, respectively. We also compared the Hα images with the HXT images. The spatial resolution of the HXT images is about $5''$. Figure 2.3 shows the time profiles in microwave, SXR, HXR, and Hα. The top solid line is that of NoRH 17 GHz, the dotted line for the GOES 1.0 - 8.0
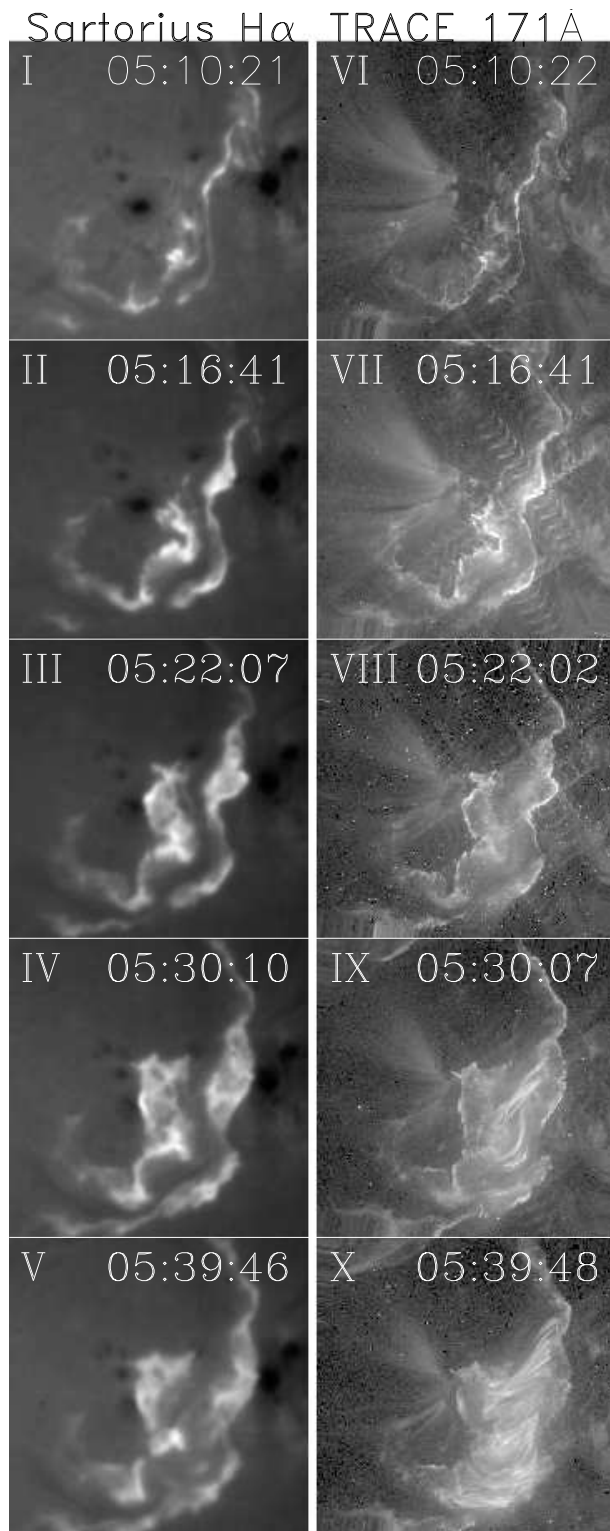
Figure 2.2: Temporal evolutions of the 2001 April 10 flare in the Hα and in the EUV. The left panels (I to V) are the Hα images obtained with the *Sartorius*. The right panels (VI to X) are the 171 Å image obtained with *TRACE*. Celestial north is up, and west is to the right.
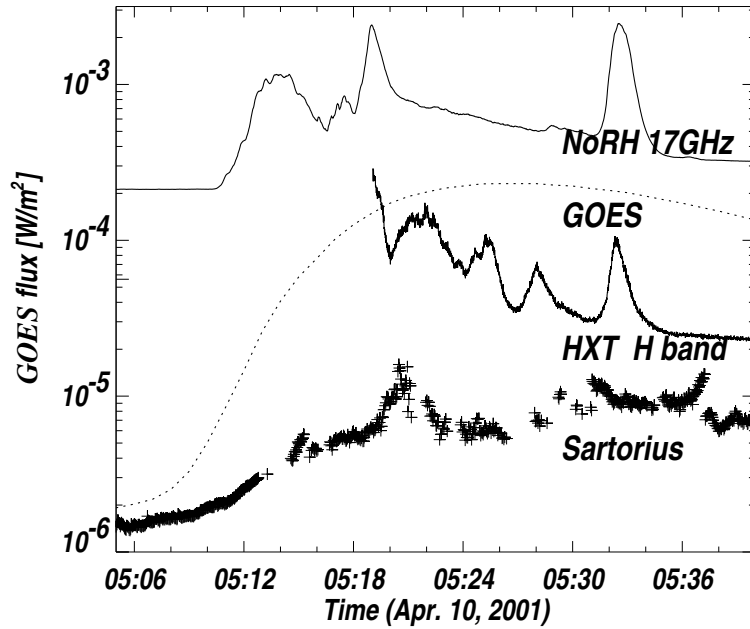
Figure 2.3: Light curves of the flare. *From top to bottom*: Radio correlation plot observed at 17 GHz with NoRH (scaled arbitrarily); soft X-ray flux in the *GOES* 1.0-8.0 Å channel (dotted line); hard X-ray count rate measured in H band (53 - 93 keV) of *Yohkoh*/HXT; and Hα obtained with *Sartorius* (plotted with plus).

Å channel, the middle solid line for the HXT H band (53 - 93 keV), and the bottom plotted line by plus sign for the total intensities of the whole Hα ribbons obtained with the *Sartorius*. The time profile of the whole Hα ribbons consists of a gradual rise and some spikes. The gradual rise feature is similar to the thermal time profile of GOES. On the other hand, spiky structure is similar to that of nonthermal profiles, like microwave and HXR as mentioned by Kurokawa, Takakura, & Ohki (1988).

2.3   Conjugate Foot Points

In this section we focus on when and where the precipitations of nonthermal particles occurred by studying in details the locations and times of the Hα brightenings. We present a new method for the analyses of the Hα brightenings (see Fig. 2.4).

2.3.1 Method of Analyses

Panel A of Figure 2.4 is an Hα image at 05:31 UT. Firstly, we divided both the flare ribbons into fine meshes (panel B). The two flare ribbons have different magnetic polarities to each other. In the panel B the left *red* mesh is positive, and the right *blue* one is negative. Each mesh box is a square with size of about 3.2 arcsec. Although this is larger than elemental Hα kernels, which are considered to be about 1 arcsec or even smaller (Kurokawa 1986), it is small enough for us to examine essentially the fine structures inside the flare ribbons. Secondly, we drew the light curves of average intensity for each box in both the meshes. We defined the "flare ribbons" as the region where the maximum intensity is more than twice of that of surrounding quiet region. The regions outside of ribbons are excluded from the analyses. Thirdly, we identified the conjugate foot points (partners), which means two foot points that show the synchronized time variation and have opposite magnetic polarities to each other. For all the boxes in ONE mesh we calculated cross-correlation functions with all boxes in THE OTHER mesh which have different magnetic polarity, and searched the highest correlated box. We performed this operation for the both flare ribbons. At the first operation performed on ONE flare ribbon, each box in the ribbon selects its own partner. After the second operation which is performed on THE OTHER mesh, if the partners which are selected in the first operation again choose the same pair as the first operation, we define this pair of points as a "highly-correlated" pair. In other words, each point of the pair selects the other point as the highest correlated point at the both operations. In panel C the *yellow* lines overlaid on panel B image are drawn to connect such highly-correlated pairs.

We examined the spatial relation between the flare loops seen in the *TRACE* 171 Å images and the highly-correlated pairs of the Hα kernels. We checked whether the Hα pairs are really connected with the 171 Å flare loops. Figure 2.5 shows the comparison of the locations of them. The Hα pairs selected above are connected with *yellow* lines. Almost all highly-correlated pairs selected above are really connected by the 171 Å flare loops, and only four pairs do not correspond to any 171 Å loops. As a result, 33 pairs were selected suitably as the foot points of the 171 Å flare loops. The good coincidence between 171 Å loops and the highly-correlated pairs of Hα kernels strongly supports the scenario of the flare loop formation: The post-flare loops seen in the *TRACE* 171 Å images are filled with the plasma evaporated at the foot points, which are the highly-correlated pairs of Hα kernels. This is an expected result, because both the foot points of flare loops are considered to appear as Hα kernels and they show high correlation
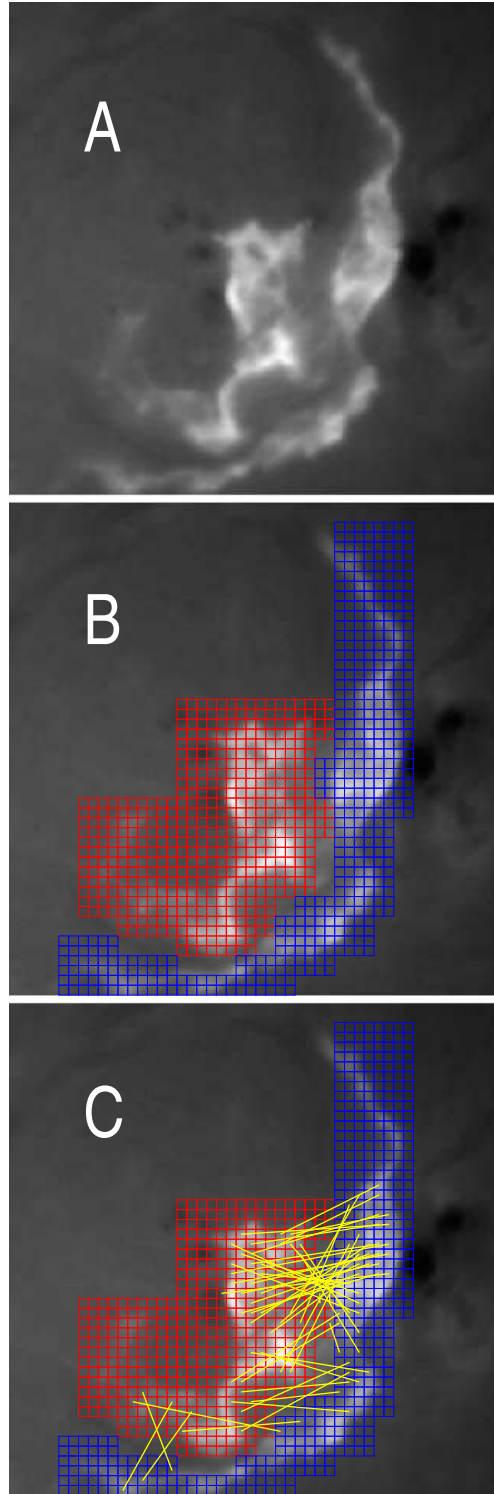
Figure 2.4: Method of data analyses. Celestial north is up, and west is to the right. Panel A is a raw Hα images of *Sartorius* at 05:31 UT. Panel B is the image overlaid with the fine meshes on panel A. The left (east) mesh drawn with *red* lines is positive polarity, and the right (west) one with *blue* lines is negative polarity. In panel C highly-correlated pairs are connected with *yellow* lines.
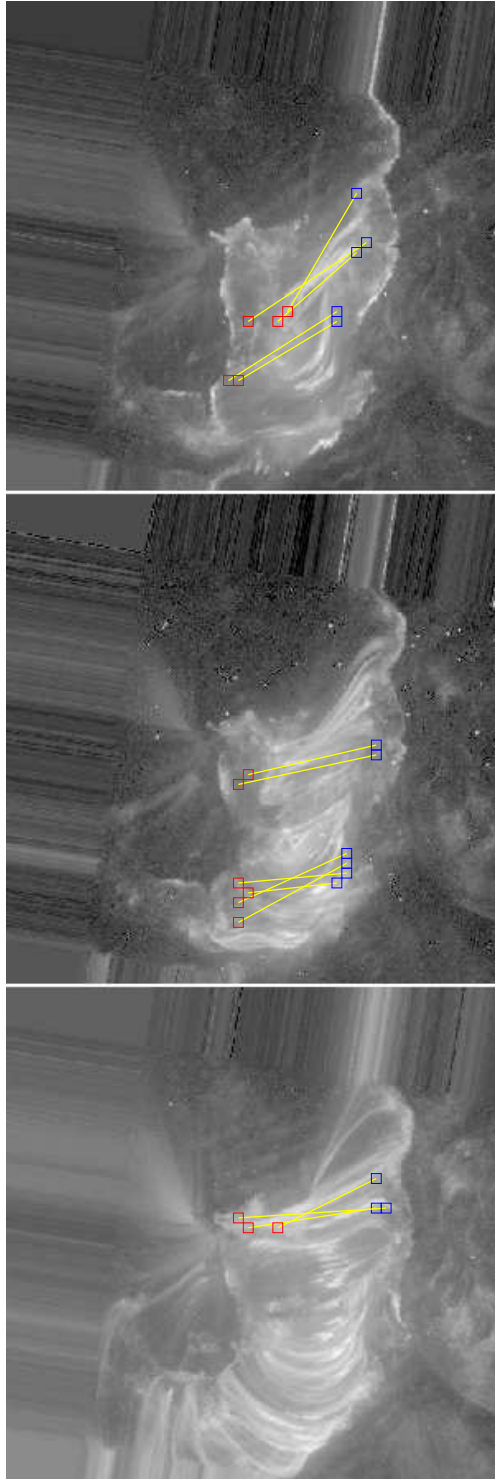
Figure 2.5: Comparison of the spatial configuration between the highly-correlated pairs of the Hα kernels and the post-flare loops seen in the *TRACE* 171 Å.

in their light curves. The spatial distribution of the Hα pairs also show the highly sheared structure at the beginning, and the more relaxed structure later.

2.3.2   Fine Structure inside Flare Ribbons

From the times and the locations of the brightenings of each highly-correlated pair of Hα kernel, we now know where and when the flare loops were connected, that is where and when the energy release occurred. These give us the informations of the site and the time of energy release, and we can follow the whole history of the energy release. Here, we examine in detail the temporal and spatial evolutions of the Hα pairs selected in §2.2.1 According to the brightening times of each pair, we classified the pairs into five groups. Figure 2.5, 2.6, 2.7, 2.8, and 2.9 show the light curves and the sites of the pairs in each group. Moreover, since the evolution of the southern part of the flare ribbons is much different from that of the northern part, we divide the Hα pairs into two parts, south and north, and examine each evolution separately.

In the southern part, the brightenings of the pairs and evolution of the flare ribbons are seen only in group 1 and 2 (see Figs. 2.6 and 2.7). The expansion of the flare ribbons appears only at the beginning of the flare. The inner part (earlier part; group 1) show impulsive rise in their light curves, while the outer part (later part; group 2) show much gradual rise. The brightenings and evolution of the flare ribbons in the northern part, on the other hand, last for longer than the southern part. First, the pairs on the innermost sides of the flare ribbons (group 1; see Fig. 2.6) have light curves with gradual rise, and their locations show tightly sheared structure same as the southern part. After that, the flare ribbons quickly separate to each other, and a lot of Hα kernels appear successively (group 2; see Fig. 2.7). Most pairs show the impulsive rise in their light curves. As the flare rather progresses, the northern flare ribbons also slow down, and the light curves of the Hα pairs show a little gradual rises (group 3; see Fig. 2.8). The locations of the pairs move to relax the shear; toward north-eastern in the eastern ribbon and south-western in the western ribbon. Even after the main expansion of the flare ribbons, other brightenings occur on the outermost sides of the ribbons. The light curves show somewhat gradual or much gradual rises (group 4 and 5; see Figs. 2.9 and 2.10, respectively). The classification is summarized in Table 2.1. Kitahara & Kurokawa (1990) reported that there are three types of Hα light curves, impulsive ones, gradual ones, and the middle ones. They also reported that the faster the flare ribbons expand, the more impulsive the light curves of Hα kernels become, and our results also agree with it.

Table 2.1: Classification of highly-correlated pairs of Hα kernels (total 33 pairs)

group	feature of light curve	number of pairs
1	. . .	10
south	impulsive	(6)
north	gradual	(4)
2	. . .	14
south	gradual	(3)
north	impulsive	(11)
3	impulsive	3
4	semi-gradual	2
5	gradual	4

The Hα pairs that belong to the same groups brighten almost simultaneously. Moreover, the brightening times of each group are responsible to each non-thermal bursts seen in HXRs and microwaves (see Figs. 2.3 and from 2.5 to 2.9). It shows that the flare ribbons expand and many Hα kernels appear while the large energy releases occur, that is the non-thermal bursts seen in HXRs and microwaves. Brightening during the valleys of the non-thermal light curves are hardly seen. This tendency is clear in group 3, 4, and 5. We can also see the tendency in group 1 and 2, though it is ambiguous because too many brightenings occur. However, even in the same group Hα pairs show a little different brightening times to each other. This shows that the energy release occur successively at the different sites during non-thermal bursts, and the successive energy release may be responsible to subpeaks seen in the bursts.

2.4 Energy Release and Evolution of Flare Ribbons

In this section we examine the relation between the evolution of the flare ribbons and the energy release during the flare. The HXR sources appear when especially large energy release occurs. Therefore, we investigate the locations and timings of the HXR sources and study what is essential for the such high energy release at the HXR sources.
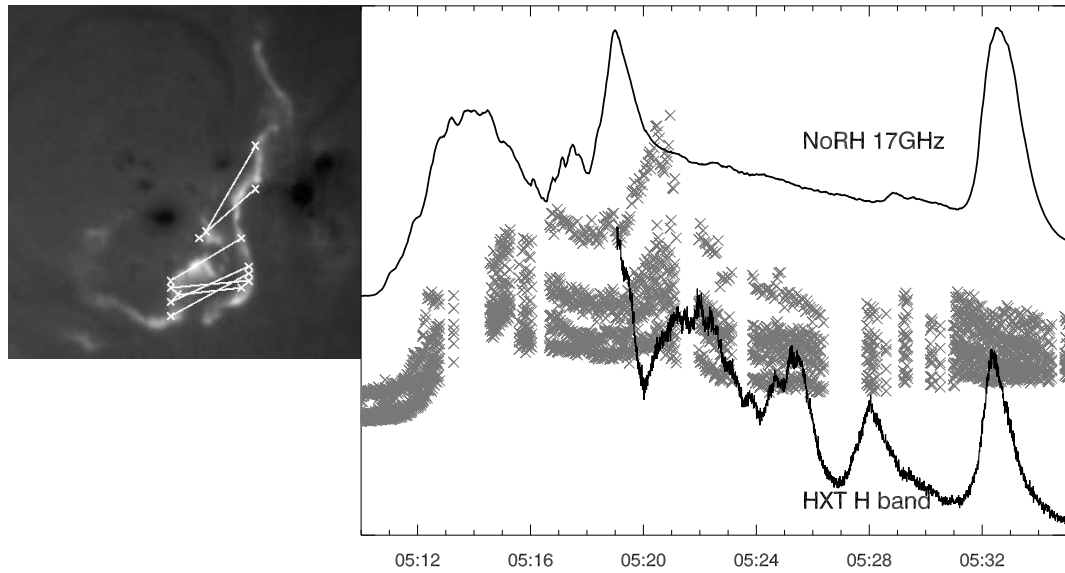
Figure 2.6: Temporal evolutions of the Hα kernels belong to group 1. *Left*: Hα images marked with the points of Hα kernels. *Right*: Gray plotted lines with crss are the light curves for kernels pointed in the left panels. Top solid line is the light curve of NoRH 17 GHz, and the bottom solid line is that of the HXT H band (53 - 93 keV).

Figure 2.7: Temporal evolutions of the Hα kernels belong to group 2.

Figure 2.8: Temporal evolutions of the Hα kernels belong to group 3.

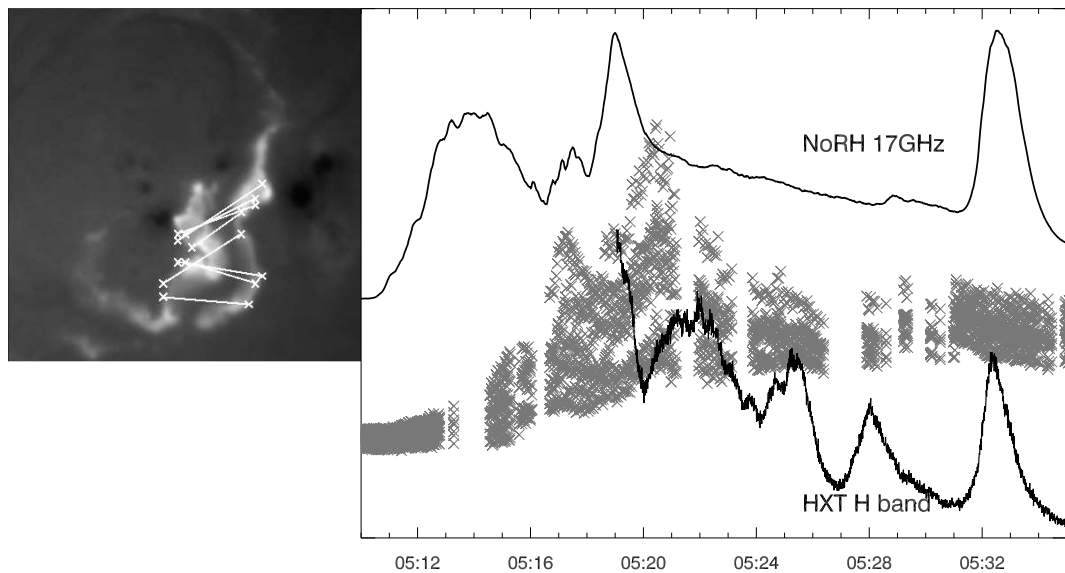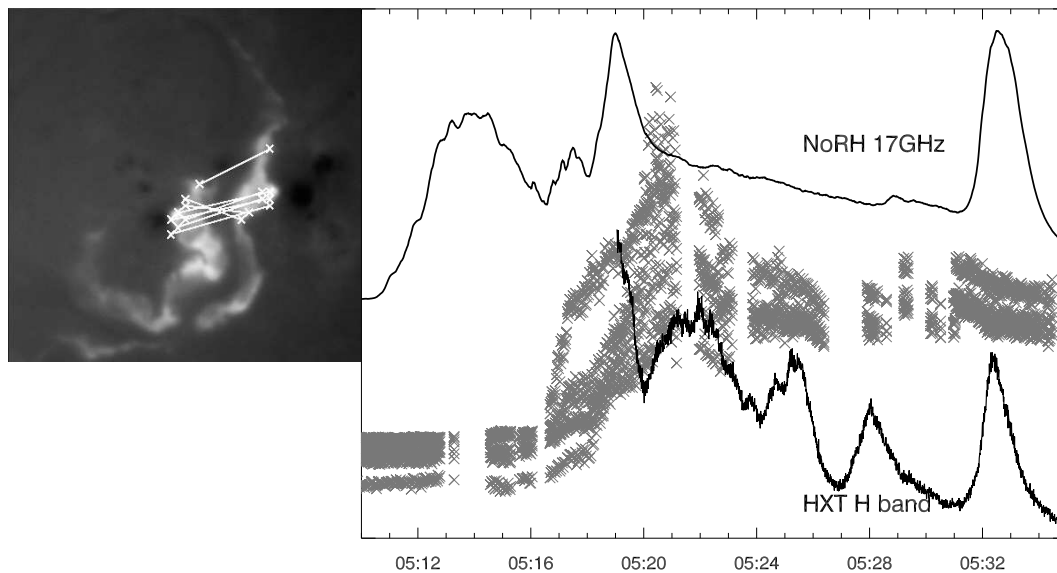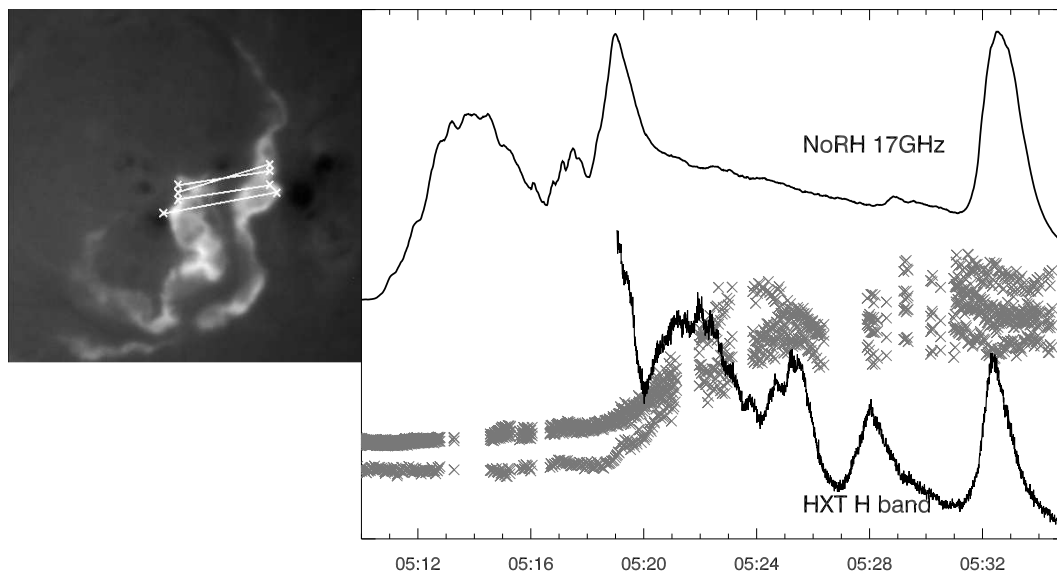Figure 2.9: Temporal evolutions of the Hα kernels belong to group 4.
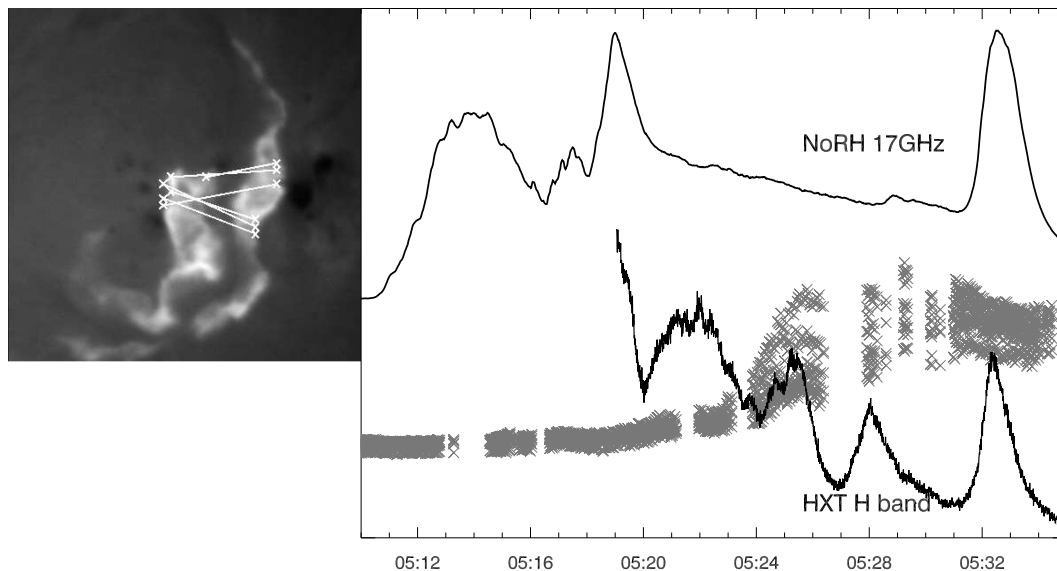
Figure 2.10: Temporal evolutions of the Hα kernels belong to group 5.

2.4.1 HXR Sources and Hα Kernels

In Hα images of flares we find a lot of brightenings evrywhere in the flare ribbons. On the other hand, HXT images show only one or two sources in them. It is known that HXR sources correspond to some Hα kernels (Sakao 1994). However, many Hα kernels are not associated with HXR sources contrary, and there are only few Hα kernels associated with HXR sources. The difference of the appearance is caused by the difference of the dynamic ranges between both the instruments. The dynamic range of HXT data is low and about 10, while that of *Sartorius* is about 200. Therefore, only the strongest sources can be seen in the HXT images, and the other weaker sources are buried in the noise. If the released energy at the HXR sources is at least 10 times larger than that at the other Hα kernels, such difference of the appearance explained. That is, the difference of the energy release must be larger than the dynamic range of the HXT data.

To examine the difference of the amount of the released magnetic energy, we measured the photospheric magnetic field strengths of each Hα kernel with the Michelson Doppler Interferometer (MDI; Scherrer *et al.* 1995) aboard *Solar and Heliospheric Observatory* (*SOHO*; Domingo *et al.* 1995). Figure 2.11 shows the Hα images at 05:19 UT. We can identify eight Hα kernels, they are actually four highly correlated pairs selected in §2.3. On the other hand, we can see only two HXR sources, which correspond to one Hα pair, E2 and W2 (marked with asterisk in Table 2.2). The yellow contour lines show HXT image. The red and blue contour lines show positive and negative
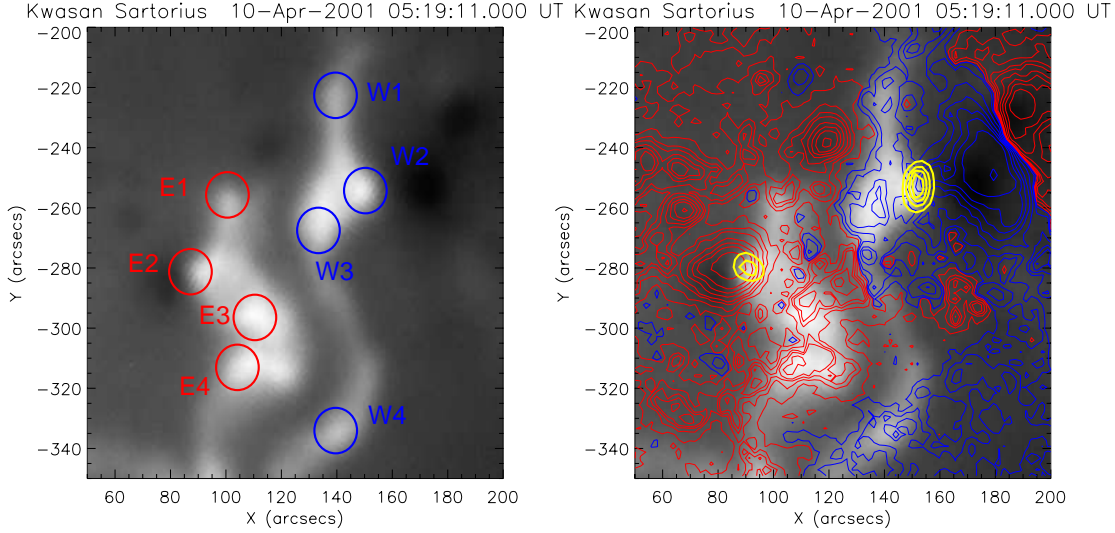
Figure 2.11: Hα image at 05:19 UT. Solar north is up, and west is to the right. *Right*; Hα image overlaid with the HXT images and *SOHO*/MDI magnetogram. The yellow contour image shows the HXT H band image. The blue and red contour lines show positive and negative polarity, respectively.

magnetic polarity taken with MDI, respectively. The Table 2.2 shows the magnetic field strengths of each kernel. The magnetic field strengths at the Hα kernels are higher than at the other regions on the average, and 400 G on the average, and those at the HXR sources are especially high ($\sim$ 1200 G). The photospheric magnetic field strength at the HXR sources is about 3 times larger than those at the other Hα kernels. This result agrees with the idea that the energy release rate in solar flares is considered to strongly depend on magnetic field strength.

Here, we assume that HXR intensity observed with HXT is proportional

Table 2.2: Magnetic Field Strength (B) of Hα Kernels

East Ribbon		West Ribbon	
Point	B (G)	Point	B (G)
E1	300	W1	-300
E2*	1350	W2*	-1200
E3	550	W3	-500
E4	500	W4	-450

* means the sources accompanied with HXR sources

to the energy release rate $\frac{dE}{dt}$ due to magnetic reconnection. The rate is proportional to the product of Poynting flux into the reconnection region and the area of the region (Isobe *et al.* 2002). The area of the reconnection region is not thought to change so much and to be independent from the magnetic field strength, then $\frac{dE}{dt} \propto B^2 v_{in}$, where B is the magnetic field density in the photosphere, v_{in} is tha inflow velocity into the reconnection region. Although magnetic field density should be defined in the corona (B_{corona}), B_{corona} is difficult to be measured, and here we assume that it is proportional to the value in the photosphere $B_{photosphere}$, and simply abbreviate to B. v_{in} has some dependence to B. The Sweet-Parker type reconnection suggests $v_{in} \propto B^{0.5}$, which is the smallest dependence. On the other hand, the largest dependence is attained at the constant reconnection rate, which means $v_{in} \propto B$. Then, dE/dt is proportional to $B^{2.5}$ to B^3. Since B at the HXR sources is 3 times larger, the energy release is 16 - 27 times stronger for Hα sources accompanied with HXR sources than for the other Hα kernels. This is sufficiently larger than the dynamic range of the HXT data, and can explain the difference of the appearance.

2.4.2   Evolution of Hα Flare Ribbons

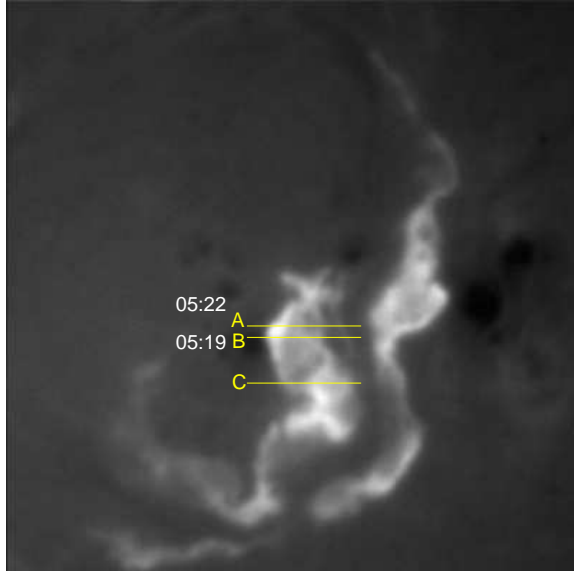
Figure 2.12: Hα flare ribbons put on the slit. Solar north is up, and west is to the right. The number of slit (A, B, and C) is common to it in Fig. 2.13. On slit A and B, the HXR sources appear at the written times.

We examined the relation between the separation of the flare ribbons and the time variation of the non-thermal radiation. The faster separation of flare ribbons to each other is considered to relate with the faster inflow into the reconnection region. Therefore, it indicates the higher inputted enegry into the reconnection site. Since the flare ribbons and the neutral line almost lie north-south direction, the evolutions of the ribbons are almost east-west direction. Therefore, we put narrow slits on the flare ribbons east-west direction, and follow the vertical, one-dimensional evolutions of the flare ribbons through the slits. Figure 2.12 shows the slits that are put on the flare ribbons. The time written in the figure shows when the HXR sources appear. The time slice images of the ribbons through the slits are given in Figure 2.13. Figure 2.13 shows three time slice images, correspond to Figure 2.12. On the slit C, there is no HXR source.

Figure 2.13 shows that the HXR sources appear when the separation of the flare ribbons decelerates. This result seems to disagree with the suggestion that the faster the flare ribbons separate, the higher energy is inputted into the reconnection region. In other words, the relation of the timings of the HXR sources with the separating speed of the flare ribbons is inverse tendency to that as expected from the above discussion.

This apparent disagreement can be solved by considering the conservation of magnetic flux. The conservation of magnetic flux is written as $B_{photosphere}v_{foot} = B_{corona}v_{inflow}$. Under the situation that $B_{photosphere}$ does not change so much, the increase of v_{foot} leads to rise of the inputted magnetic flux into the reconnection region as expected. On the other hand, if $B_{photosphere}$ rapidly increases and the inputted magnetic flux does not change, v_{foot} decreases. In the flare as the flare ribbons separate to each other, they approach to the sunspot umbrae, and the magnetic field strengths rapidly increase. Therefore, the separation of the flare ribbons slow down quickly. As we mentioned in §2.4.1, the HXR sources appear at the high magnetic field strength points. The apparent disagreement is explained with the rapid increase of $B_{photosphere}$. The effect of magnetic field works more strongly than the separation of the flare ribbons.
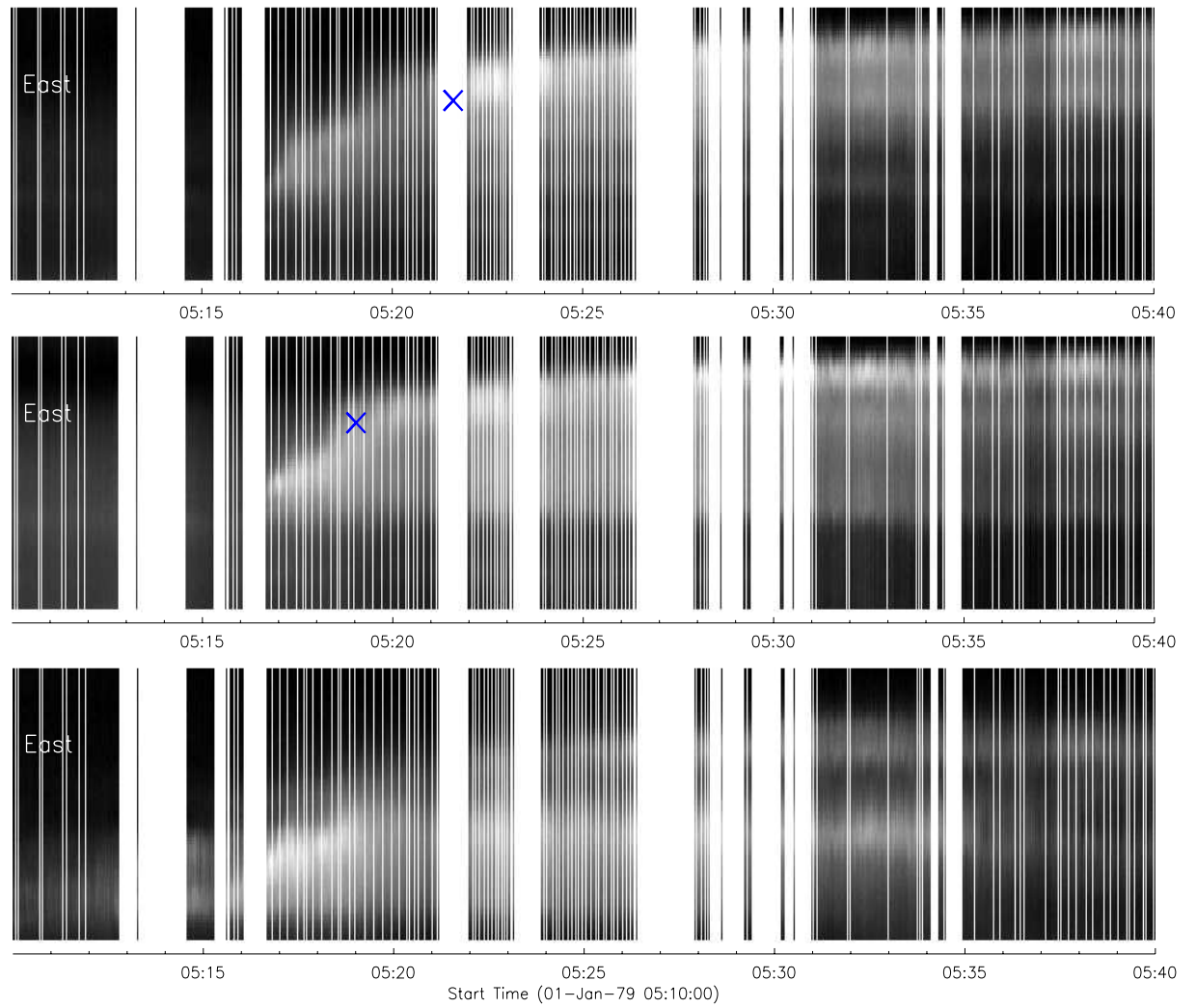
Figure 2.13: Time slice images of the Hα flare ribbons. The HXR sources locate on the points marked with blue cross. The vertical axis shows the distance from the neutral line, and the horizontal axis is the time.

2.5   Summary and Discussion

We examined in detail the temporal and spatial evolution of the Hα kernels with a unique method. We first identified the conjugate foot points in both the flare ribbon with different magnetic polarities by calculating crosscorrelation factors of the light curves of each Hα kernel. We second confirmed whether the highly-correlated pairs of Hα kernels are really connected with the post-flare loops seen in the *TRACE* 171 Å images. Then, we have been able to followed the whole history of the energy release.

The flare showed that the steepness of the Hα light curves, impulsive rise and gradual rise, clearly relates to the separating speed of the flare ribbons. According to the conservation of magnetic flux, the magnetic flux swept with the flare ribbons is equal to the amount that inputted into the site of magnetic reconnection. Therefore, the faster the flare ribbons separate, the higher the magnetic energy inputs to the flare. We need to investigate in more detail the relation between the type of light curves and the amount of energy release. For example, the difference of evolution of the flare ribbons between in the south and in the north may show the difference of the amount and/or the mechanism of energy release. The difference of the thickness of the flare ribbons which may be caused by the initial global magnetic field, the difference of magnetic field strength, and so on are suggested as factors that cause such a difference of the energy release. These will be studied in our future paper.

The global distribution of highly-correlated pairs of Hα kernels implies as a whole the emergence of twisted magnetic flux bundles (Ishii, Kurokawa, & Takeuchi 2000). The Hα pairs move to relax the sheared structure. The post-flare loops seen in the *TRACE* 171 Å images also show the tightly sheared structure in the beginning, then larger and more relaxed structure. In other words, the large and relaxed configuration of magnetic field lie on the inner sheared structure. It may be caused by the emergence of tightly twisted flux tubes and their relaxations (Ishii, Kurokawa, & Takeuchi 2000).

The brightenings of the Hα pairs that belong to the same group occur almost simultaneously. It shows that although we may miss the tiny brightenings that occur at valleys of non-thermal light curves, the energy input to the flare loops occur almost simultaneously over a wide region during such large energy releases that generate non-thermal bursts. The Hα pairs that belong to the same group, which means are responsible to the same non-thermal bursts, show a little different times of brightening to each other. Each brightening may be correspond to each subpeak seen in the non-thermal bursts.

We have found that the magnetic field strengths at the HXR sources are

rather higher than at the other Hα kernels. The magnetic field strength largely affects the amount of the energy release. On the other hand, the HXR sources appear when the flare ribbons decelerates. Although the deceleration of the flare ribbons shows the low inputted energy into the reconnection site apparently, the magnetic field strengths rapidly increase at the foot points, then the HXR sources appear. To make clear the time variation of energy release affected with the environments needs more detailed studies by considering both the magnetic field strength and the separation speed simultaneously, e.g., the time variation of Poynting flux and/or reconnection rate.

Bibliography

Domingo, V., Fleck, B., & Poland, A. I., 1995, Solar Phys., 162, 1

Handy, B. N., et al., 1999, Solar Phys., 187, 229

Ishii, T. T., Kurokawa, H., & Takeuchi, T. T., 2000, Publ. Astron. Soc. Japan, 52, 337

Isobe, H., et al., 2002, Astrophys. J., 566, 528

Kitahara, T., Kurokawa, H., 1990, Solar Phys., 125, 321

Kosugi, T., et al., 1991, Solar Phys., 136, 17

Kurokawa, H., 1986, Low Atmosphere of Solar Flares (ed. D. Neidig), Proc. of the SMM Symp., Sunspot, NM, National Solar Observatory, p. 51

Kurokawa, H., Takakura, T., Ohki, K., 1988, Publ. Astron. Soc. Japan, 40, 357

Kurokawa, H., Kawai, G., Kitai, R., Funakoshi, Y., Nakai, Y., Tsuneta, S., Acton, and L. W., Ogawara, Y., 1992, Publ. Astron. Soc. Japan, 44, 129

Ogawara, Y., Takano, T., Kato, T., Kosugi, T., Tsuneta, S., Watanabe, T., Kondo, I., and Uchida, U., 1991, Solar Phys., 136, 10

Qiu, J., Ding, M. D., Wang, H., Gallagher, P. T., Sato, J., Denker, C., & Goode, P. R., 2001, Astrophys. J., 554, 445

Sakao, T., 1994, Ph.D. thesis (University of Tokyo)

Scherrer, P. H., et al., 1995, Solar Phys., 162, 129

Schrijver, C. J. et al., 1999, Solar Phys., 187, 261

Trottet, G., Rolli, E., Magun, A., Barat, C., Kuznetsov, A., Sunyaev, R., & Terekhov, O., 2000, A&A, 356, 1067

Tsuneta, S., et al., 1991, Solar Phys., 136, 37

Wang, H., Qiu, J., Denker, C., Spirock, T., Chen, H., & Goode P. R., 2000, Astrophys. J., 542, 1080

Chapter 3

Periodic Acceleration of Electrons[*]

We present an examination of the multiwavelength observation of a C7.9 flare that occurred on 1998 November 10. This is the first imaging observation of the quasi-periodic pulsations (QPPs). Four bursts were observed with the hard X-ray telescope aboard *Yohkoh* and the Nobeyama Radioheliograph during the impulsive phase of the flare. In the second burst, the hard X-ray and microwave time profiles clearly showed a QPP. We estimated the Alfvén transit time along the flare loop using the images of the soft X-ray telescope aboard *Yohkoh* and the photospheric magnetgrams and found that the transit time was almost equal to the period of the QPP. We therefore suggest, based on a shock acceleration model, that variations of macroscopic magnetic structures, such as oscillations of coronal loops, affect the efficiency of particle injection/acceleration.

3.1   Introduction

Non-thermal electrons generated in the impulsive phase of a flare are observed in hard X-rays, γ-rays, and microwaves. The light curves in these wavelengths show short-lived bursts with durations between 10 s and 10 minutes (Dulk, McLean, & Nelson 1985). These bursts include smaller pulses with shorter duration, and they sometimes show periodicity.

A good example of such quasi-periodic pulsations (QPPs) was seen in a flare on 1980 June 7 (Kiplinger et al. 1983). Nakajima et al. (1983) and

---

[*]This chapter was published in Astrophys. J., 2001, 562, L103, entitled "Periodic Acceleration of Electrons in the 1998 November 10 Solar Flare" by Asai, A., Shimojo, M., Isobe, H., Morimoto, T., Yokoyama, T., Shibasaki, K. and Nakajima, H.

Kane et al. (1983) examined the temporal evolution of the X-ray and radio spectra and the spatial structure of the flare. They suggest that the quasi-periodic pulses indicate a modulation of the particle injection/acceleration rate. Tajima, Brunel, & Sakai (1982) showed by numerical simulation that stored magnetic energy is explosively transformed to particle acceleration. They also suggest that the current loop coalescence instability induces the QPPs. Moreover, Tajima et al. (1987) showed that the period of the QPP is equal to the Alfvén transit time "across" the current loop. However, these works were mainly based on the total flux, and the detailed spatial configuration of the flare that shows QPP is still unknown.

On 1998 November 10 a solar flare (C7.9 on the *GOES* scale) occurred in NOAA Active Region (AR) 8375. The flare was observed by *Yohkoh* (Ogawara et al. 1991) and the Nobeyama Radio Observatory and clearly showed quasi-periodic behavior in the hard X-ray and microwave time profiles. In this chapter, we analyze the QPP using the high-resolution X-ray and microwave images. Then we compare the period of the QPP with typical timescales of flare loops. Finally, we discuss the effect of the magnetic structure on the particle injection/acceleration rate.

3.2   Observations

The solar flare occurred in NOAA AR 8375 (N19°, W78°) at 00:10 UT, 1998 November 10. Microwave images of the flare were taken with the Nobeyama Radioheliograph (NoRH; Nakajima et al. 1994), which observed the sun at 17 and 34 GHz with a temporal resolution of 1.0 s. The spatial resolutions of NoRH data are 12″ for 17 GHz and 6″ for 34 GHz. The Nobeyama Radio Polarimeter (NoRP; Torii et al. 1979; Shibasaki et al. 1979; Nakajima et al. 1985) measured the total flux of the flare at 1, 2, 3.75, 9.4, 17, 34, and 80 GHz with a temporal resolution of 0.1 s. The hard X-ray images were obtained with the hard X-ray telescope (HXT; Kosugi et al. 1991) aboard *Yohkoh*, with a spatial and temporal resolution of about 5″ and 0.5 s, respectively. The soft X-ray images were also obtained with the *Yohkoh* soft X-ray telescope (SXT; Tsuneta et al. 1991). We used full-resolution images in the partial frame image mode with a spatial resolution of about 2″.5.

Figure 3.1 shows the microwave, soft X-ray, and hard X-ray time profiles. The top solid line is that of the NoRH 17 GHz, the dotted line is the *GOES* 1.0 - 8.0 Å channel, the middle solid line is the HXT M1 band (23 - 33 keV), and the bottom solid line is the HXT L band (14 - 23 keV). Four bursts with duration between 10 and 30 s are seen in the microwave and hard X-ray emission. The fine spikes in the second burst clearly show the QPPs
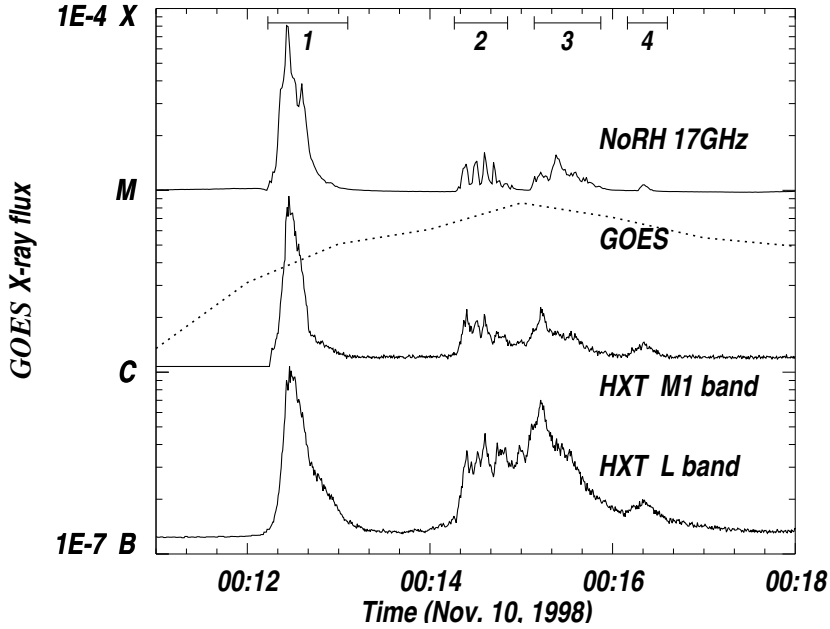
Figure 3.1: Temporal evolution of the 1998 November 10 flare. *From top to bottom*: Radio correlation plot observed at 17 GHz with NoRH (scaled arbitrarily); soft X-ray flux in the *GOES* 1.0 - 8.0 Å channel (*dotted line*); and hard X-ray count rate measured in the M1 band (23 - 33 keV) and L band (14 - 23 keV) of *Yohkoh*/HXT (scaled arbitrarily). Four bursts are identified by the numbered top bars.

in both microwaves and hard X-rays. In this chapter, we investigate the quasi-periodic nature of the second burst.

Figure 3.2 shows the images of NoRH/17 GHz, the HXT/M1 band, and the SXT at the second burst. The flare shows a double source in the microwave data (*gray contours*). We refer to the northern and brighter source as the "source A" and the other one as "source B". On the other hand, in the hard X-ray data (*black contours*) only one source is seen near source B. This is common in the L and M1 bands of HXT, but it is unknown whether it is also common in the M2 (33 - 53 keV) and H (53 - 93 keV) bands. We could not synthesize the hard X-ray images in these bands at the time due to insufficient counts. The soft X-ray image (*gray scale*) shows a small bright kernel at the same region at source B. We can also see a faint loop that connects the bright kernel and the radio source A.
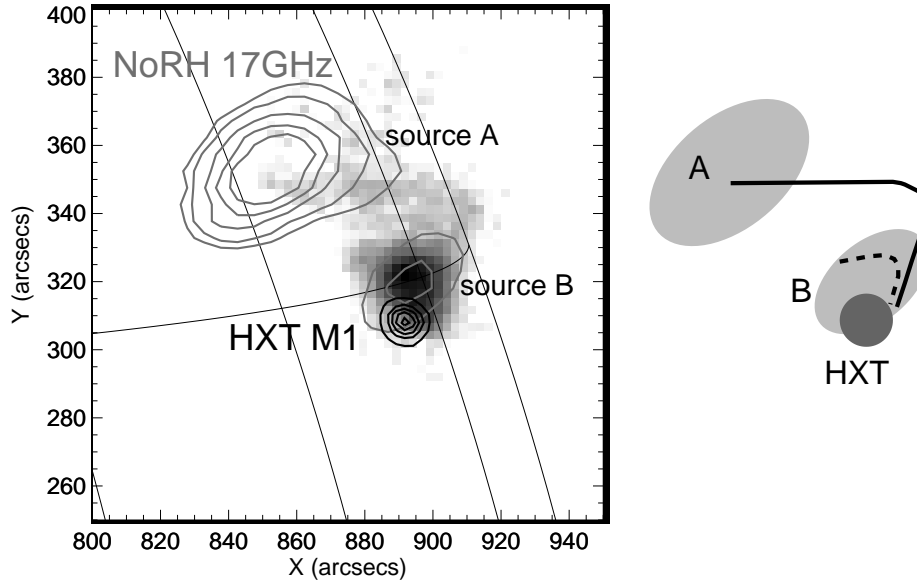
Figure 3.2: *Left*: Co-aligned images of the flare. SXT (Be filter) image is shown by the gray scale at 00:14:32 UT. NoRH (17 GHz; *gray contour*) image of 00:14:37 UT is plotted at brightness temperatures of 150,000, 200,000, 300,000, 400,000, and 500,000 K. HXT (M1 band, 23 - 33 keV) image at 00:14:33 UT is drawn as the black contour. Contour levels are 90%, 70%, 50%, 30%, and 10% of the peak intensity. *Right*: Simple sketch of this region. The NoRH sources, the HXT source, and SXT faint loop are displayed in light gray, dark gray, and a black solid line, respectively. There probably are flare loops (*dashed line*; see §3.3) in microwave source B.

3.3   Periodic Pulsation

Figure 3.3 presents the hard X-ray and microwave time profiles for the second burst, from 00:14:20 UT to 00:14:40 UT. The QPPs are clearly seen. In the time profiles obtained with the NoRP data, the QPPs are seen in 9.4 and 17 GHz. The period calculated from the autocorrelation function of the time profiles was 6.6 s. We also calculated the period of the QPPs in hard X-rays (M1 and M2 bands) and found that the period (6 s) was almost the same as those in NoRP. We analyzed the microwave spectrum using the NoRP data and found that the power-law distribution index was about -2 to -1.5 and the turnover frequency was about 10 GHz. These results indicate that the emission of the QPP originated from gyrosynchrotron radiation from non-
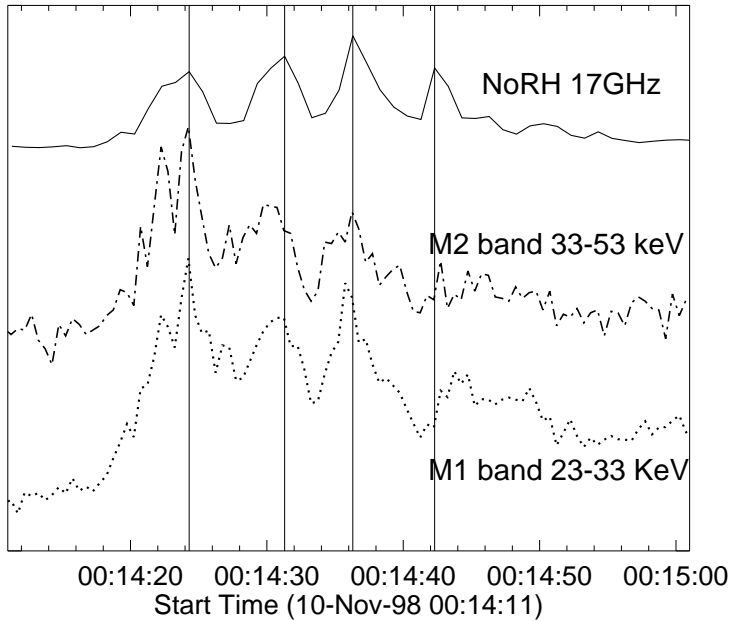
Figure 3.3: Light curves of the second burst (scaled arbitarily). From top to bottom: radio brightness temperature observed at 17 GHz by NoRH (*solid line*); hard X-ray count rate measured in the M2 band (33 - 53 keV) (*dash dot line*) and M1 band (23 - 33 keV) (*dotted line*) of *Yohkoh*/HXT. The vertical lines show the peak times of the microwave emission.

thermal electrons. Since both the time profiles of the M1 and M2 bands clearly showed the QPPs, the emission in hard X-rays was also produced by non-thermal electrons.

As described in §3.2, the flare has two microwave sources (see Fig. 3.2). We found that the time profile of source A showed the QPP, while that of source B did not. The pulsating source is different from the hard X-ray source that is located near source B. To clarify the relation between the microwave pulsation at source A and the hard X-ray pulsation, we calculated the correlation between the time profiles of 17 GHz and the M1 band as a function of the time lag between them. The maximum correlation was found for a delay of the microwave pulsation with a time of 0.6 – 1.0 s.

We suggest that the acceleration site lies near the hard X-ray source and that the delay time between microwaves and hard X-rays is explained by the flight duration of non-thermal electrons between both the sources. The length of the soft X-ray faint loop connecting the hard X-ray source and source A is about 5.0×10^4 km. If we assume that the velocity of the

electrons is about 1.0×10^5 km s^{-1} (~ 30 % of the speed of light), the delay time between microwaves and hard X-rays is about 0.5 s, which is almost equal to the observed delay time. The soft X-ray images show two parts related to the flare: a bright kernel near source B and a faint large loop connecting the kernel and source A (see Fig. 3.2). We believe that the flare occurred at the contact region of the two parts via magnetic reconnection (Hanaoka 1997; Heyvaerts, Priest, & Rust 1977). In such a scenario, the acceleration site would be located near the reconnection site. Hence, it is reasonable to suggest that the acceleration site is located near source B and the hard X-ray source.

Here, another question occurs: Why did the time profile of the microwave source B not show the QPP? As an answer, we suggest that the emission mechanism of source B differs from that of source A. The emission mechanism of source A is optically thin gyrosynchrotron radiation from non-thermal electrons. On the other hand, the dominant emission mechanism of source B is optically thin thermal bremsstrahlung since the spectrum index of source B that is derived from the 17 and 34 GHz is about 0. Therefore, the time profiles of source B do not show the population of the accelerated/injected non-thermal electrons. To confirm the suggestion, we estimated the thermal radio flux from source B by using the temperature and the emission measure of the SXT bright kernel (see §3.4), and found that the flux was almost the same as the observed flux of source B. We also suggest that the thermal emission was radiated from the thermal plasma that was confined by the flare loops. The loops were formed at the first burst via magnetic reconnection. Therefore, although the fine structure of the kernel is not resolved in the SXT images, we think that it consists of the main flare loops (see Fig. 3.2).

3.4   Typical Timescales of the Flare Loop

In §3.3, we showed that the period of the pulsation was 6.6 s. What is the explanatin for the period? To answer the question, we derive some typical timescales of the flare loop and discuss them. Temperature, density, size, and magnetic field strength of the flare loop are needed for the estimation. The temperature T and the volume emission measure EM are derived from the soft X-ray images that were taken with the SXT thick aluminum (Al12) and beryllium (Be) filters. The region of flare loop A is defined as the region where the intensity of an SXT Be filter image is more than 2000 DN s^{-1} pix^{-1}. This leads to an area of 2.5×10^{18} cm^2. Using the filter ratio method (Hara et al. 1992), the average temperature and volume emission measure over the flare loop are calculated to be 9.4 MK and 8.1×10^{48} cm^{-3}, respectively.

Here, we assume that the kernel is a cube, and that the volume V of the flare kernel is the area to the power of three halves, i.e., $V = A^{3/2}$. Then, the number density n in the top of the flare loop becomes $n = (EM/V)^{1/2} = (EM/A)^{3/2} \approx 4.5 \times 10^{10}$ cm^{-3}. Also, the acoustic velocity c_s in the flare loop is given by $c_s \approx (\gamma k_B T/m_p)^{1/2} \approx 360$ km s^{-1}, where k_B is Boltzmann's constant, m_p is the proton mass, and γ is the ratio of specific heats and is here assumed to be 5/3. Since the structure of the flare loop is not resolved in the SXT images, we can not measure the length l and width w of the flare loop correctly. Therefore, we use the square root of the area instead of the length of the flare loop ($l \sim A^{1/2} \sim 16{,}000$ km). Then, the acoustic transit time "along" the flare loop is $\tau_{s,l} = l/c_s \approx 44$ s. On the other hand, if we use the width of the faint loop instead of the width of the flare loop ($w \sim 6000$ km), the acoustic transit time "across" the flare loop becomes $\tau_{s,w} = w/c_s \approx 17$ s. Both the timescales are much longer than the observational period of the QPP (6.6 s).

In order to derive the Alfvén transit times of the flare loop, we have to estimate the magnetic field strength in the corona. However, this estimation is difficult in our case as (1) we cannot measure the magnetic field strength of the corona directly, and (2) we cannot obtain the actual magnetic field strength in the photosphere at the flare region since it is located near the north-west limb. Therefore, we calculate the potential field of the flare region based on a magnetogram on November 6. The magnetogram was obtained with the Michelson Doppler Interferometer (MDI; Scherrer et al. 1995) aboard the *Solar and Heliospheric Observatory* (*SOHO*; Domingo, Fleck, & Poland 1995). The field strength on the apex of the flare loop B is estimated to be about 300 G using the potential field extrapolation by the software package MAGPACK2 (Sakurai 1982). As a result, the Alfvén velocity c_A in the flare loop becomes $c_A \approx B/(4\pi n m_p)^{1/2} \approx 3100$ km s^{-1}. Then, the Alfvén transit time "along" the flare loop is $\tau_{A,l} = l/c_A \approx 5.1$ s and the Alfvén transit time "across" the flare loop is $\tau_{A,w} = w/c_A \approx 1.9$ s.

The values of our estimations are summarized in Table 3.1. Although the Alfvén transit time is sensitive to the magnetic field strength estimated above, the transit time along the flare loop ($\tau_{A,l}$) is the most similar to the observational period of the pulsation in microwaves and hard X-rays.

3.5 Discussion

We investigated the impulsive phase of the flare whose time evolution showed a clear QPP in microwaves and hard X-rays. We found that the periods of the QPP were 6.6 s and that the acceleration site of non-thermal electrons was

Table 3.1: Physical Values of Flare Loop

Parameter	Value
Area (A)	2.5×10^{18} cm^2
Volume (V)	4.0×10^{27} cm^3
Length (l)	1.6×10^9 cm
Width (w)	$\sim 6.0 \times 10^8$ cm
Temperature (T)	9.4×10^6 K
Number density (n)	4.5×10^{10} cm^{-3}
Magnetic field (B)	~ 300 G
Acoustic velocity (c_s)	3.6×10^2 km s^{-1}
Alfvén velocity (c_A)	3.1×10^3 km s^{-1}
Acoustic transit time:	
along the loop $(\tau_{s,l})$	44 s
across the loop $(\tau_{s,w})$	17 s
Alfvén transit time:	
along the loop $(\tau_{A,l})$	5.1 s
across the loop $(\tau_{A,w})$	1.9 s

located near source B using correlation analysis of the time profiles. Then, we estimated some typical timescales of the flare loop from the observational data and found that the Alfvén transit time along the flare loop was close to the period of the pulsation.

Tajima et al. (1987) suggest that the periods of QPP in microwaves and hard X-rays are equal to an Alfvén transit time across the flare loop $(\tau_{A,w})$. However, this transit time was much shorter than the observational period of the QPP. This implies that the origin of the periodic pulsation in our case is not the coalescence instability in the reconnection site.

Recently, *Transition Region and Coronal Explorer* (Handy et al. 1999) observations have shown coronal loop oscillations that was induced by a flare (Nakariakov et al. 1999). T. Miyagoshi (in preparation) performed three-dimensional MHD simulations of the coronal loop oscillation and found that the period of the loop oscillation is equal to the Alfvén transit time along the oscillating loops $(\tau_{A,l})$. Does the oscillation of the coronal loop relate with the particle acceleration/injection? Tsuneta & Naito (1998) propose that non-thermal electrons can efficiently be accelerated by a first-order Fermi process at the fast shock located below the reconnection X-point. They suggest that the accelerated electrons are trapped between the two slow shocks and that the energy injection depends on the length of the fast shock which is

pinched by these slow shocks. If the reconnected (flare) loop that is located under the fast shock is oscillating, that the length of the fast shock probably varies with the loop oscillation, synchronously. Hence, we propose, under the hypothesis of the acceleration model proposed by Tsuneta and Naito (1998), that the origin of the QPP in microwaves and hard X-rays is the modulation of the acceleration/injection of non-thermal electrons. Moreover, we propose that the modulation is produced by the variations of macroscopic magnetic structures, for example, oscillations of coronal loops.

Bibliography

Domingo, V., Fleck, B., and Poland, A. I., 1995, Solar phys., 162, 1

Dulk, G. A., McLean, D. J., & Nelson, G. J., 1985, Solar Radiophysics: Studies of emission from the sun at metre wavelengths, ed.s McLean D. J. & Labrum N. R. (Cambridge: Cambridge University Press), 53

Hanaoka, Y., 1997, Solar phys., 173, 319

Handy, B. N., et al., 1999, Solar phys., 187, 229

Hara, H., Tsuneta, S., Lemen, J. R., Acton, L. W., and McTiernan, J. M., 1992, Publ. Astron. Soc. Japan, 44, 135

Heyvaerts, J., Priest, E. R., and Rust, D. M., 1977, Astrophys. J., 216, 123

Kane, S. R., Kai, K., Kosugi, T., Enome, S., and Landecker, P. B., & McKenzie, D. L., 1983, Astrophys. J., 271, 376

Kiplinger, A. L., Dennis, B. R., Frost, K. J., & Orwig, L. E., 1983, Astrophys. J., 273, 783

Kosugi, T., et al., 1991, Solar phys., 136, 17

Nakajima, H., Kosugi, T., Kai, K., & Enome, S., 1983, Nature, 305, 292

Nakajima, H., et al., 1985, Publ. Astron. Soc. Japan, 37, 163

Nakajima, H., et al., 1994, in Proc. of the IEEE, 82, 705

Nakariakov, V. M., Ofman, L., DeLuca, E. E., Roberts, B., & Davila, J. M., 1999, Science, 285, 862

Ogawara, Y., Takano, T., Kato, T., Kosugi, T., Tsuneta, S., Watanabe, T., Kondo, I., & Uchida, Y., 1991, Solar phys., 136, 10

Sakurai, T., 1982, Solar phys., 76, 301

Scherrer, P. H., et al., 1995, Solar phys., 162, 129

Shibasaki, K., Ishiguro, & M., Enome, S., 1979, in Proc. of the Res. Inst. of Atmospherics, Nagoya Univ., 26, 117

Tajima, T., Brunel, F., and Sakai, J., 1982, Astrophys. J., 258, L45

Tajima, T., Sakai, J., Nakajima, H., Kosugi, T., Brunel, F., & Kundu, M. R., 1987, Astrophys. J., 321, 1031

Torii, C., Tsukiji, Y., Kobayashi, S., Yoshimi, N., Tanaka, H., Enome, S., 1979, in Proc. of the Res. Inst. of Atmospherics, Nagoya Univ., 26, 129

Tsuneta, S., et al., 1991, Solar phys., 136, 37

Tsuneta, S., and Naito, T., 1998, Astrophys. J., 495, L67

Chapter 4

Plasma Ejections from a Light Bridge in a Sunspot Umbra**

We present conspicuous activities of plasma ejections along a light bridge of a stable and mature sunspot in NOAA Active Region 8971 on 2000 May 2. We found the ejections both in the Hα (10^4 K) images obtained with the Domeless Solar Telescope at Hida Observatory and in the 171 Å (Fe IX/X; $\sim 10^6$ K) images obtained with the *Transition Region and Coronal Explorer*. Main characteristics of the ejections are as follows: (1) Ejections occur intermittently and recurrently. (2) The velocities and the timings of the 171 Å ejections are the same as those of Hα ejections. (3) The appearance of ejections are different from one another; i.e., the Hα ejections have jetlike appearance, while the 171 Å ejections are like loops.

4.1   Introduction

Characteristics of Hα surges have been studied for many years (e.g., Roy 1973) and are summarized by Bruzek & Durrant (1977) as follows: (1) Hα surges are straight or slightly curved spikes that are shot out of a small mound. (2) On the solar disk, they appear usually in absorption, but in their initial phase, sometimes in emission. (3) They also show strong tendency to recur. Kurokawa (1988) and Kurokawa & Kawai (1993) have reported that Hα surges are often found at the earliest stage of emerging flux regions (EFRs) and continue recurrently for many hours. They have also suggested that magnetic reconnection between a newly emerging flux and a

---

**This chapter was published in Astrophys. J., 2001, 555, L65, entitled "Plasma Ejections from a Light Bridge in a Sunspot Umbra" by Asai, A., Ishii, T. T. and Kurokawa, H.

pre-existing magnetic field is the essential mechanism of Hα surge production. Yokoyama & Shibata (1995) showed in their numerical simulation that such a reconnection really produces Hα surges in EFRs.

Roy (1973) found that Hα surges are also ejected from a light bridge of a sunspot umbra. However, no detailed study has been made of plasma ejections from a light bridge until now. We use the term "light bridge" to refer to a bright, long, and narrow feature penetrating or crossing a sunspot umbra. Light bridges are often seen in umbrae of mature and stable sunspots and have been considered to have the same magnetic polarity as that of the sunspot umbrae, while their field strength is much weaker (Beckers & Schröter 1969).

We found that conspicuous Hα surge activities occurred along the light bridge of the sunspot umbra in the NOAA Active Region (AR) 8971 on 2000 May 2, with 60 cm Domeless Solar Telescope (DST) at Hida Observatory, Kyoto University. Hα surge activities continued intermittently for about 6.5 hr, as long as the time span of our observation. Examining the extreme-ultraviolet (EUV) images obtained with the *Transition Region and Coronal Explorer* (*TRACE*; Handy et al. 1999; Schrijver et al. 1999), we found similar ejections from the light bridge in 171 Å (Fe IX/X) images. Such ejections from a light bridge have never been reported before in the EUV wavelength. From now on, we refer to the ejection seen in 171 Å images obtained with *TRACE* as "171 Å ejection".

In this Chapter, we report the morphological and the dynamical characteristics of the ejections from the light bridge, using the Hα and the 171 Å images of high spatial and temporal resolution obtained with DST and *TRACE*, respectively. In §4.2, we summarize the observational data, and in §4.3, we present observational results and discussion. In §4.3.1, we report the features of the Hα surges obtained with DST, and in §4.3.2, compare them with 171 Å ejections. Then we discuss the magnetic configuration of this region and possible mechanisms for the surge activity in the light bridge in §4.3.3. Our results are summarized in §4.4.

4.2   Observational Data

We have observed the surge activities along the light bridge in the NOAA AR 8971 (N20° , W55°) with DST from 23:00 UT on 2000 May 1 to 05:30 UT on May 2. The Hα monochromatic images were obtained with the Zeiss Lyot filter of 0.25 Å passband and SONY laservideo disc recorder sequentially in 3 wavelengths: H$\alpha \pm 0.0$, $+0.6$, and -0.6 Å. The successive wavelength change and recording were controlled with a personal computer, and the
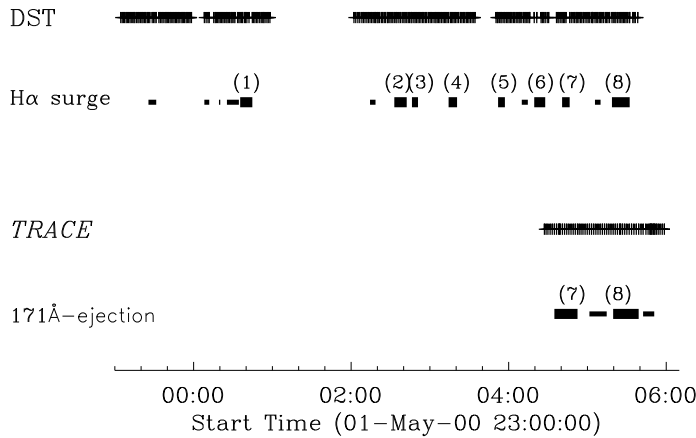
Figure 4.1: Schematic description of the observation log. Each observed time is represented by plus sign. The second and the fourth rows show the ejections seen in the Hα images and in the EUV images, respectively. Ejections in both the Hα and 171 Å occur recurrently.

time capture for each wavelength was 12 s. In this study we mainly used the Hα − 0.6 Å images, in which their ejecting motions are clearly seen.

The EUV images of this region obtained with *TRACE* are available from 04:30 UT to 06:00 UT on May 2. They also show conspicuous ejections along the light bridge. The *TRACE* 171 Å images were used to compare the features of the hot ejections of about 10^6 K with those of Hα cool surges of about 10^4 K. To co-align the Hα images with the EUV images, we used a *TRACE* 1600 Å image. There are a few soft X-ray images obtained with the soft X-ray telescope (SXT) aboard *Yohkoh* (Tsuneta et al. 1991) during the time interval from 05:20 UT to 05:30 UT on May 2. To process the *TRACE* and *Yohkoh* SXT images, we used the Interactive Data Language solar software.

In Figure 4.1, the times of Hα and EUV observations are summarized, where each time is represented by plus sign. The second and fourth rows show the times when the ejections along the light bridge are distinctly identified at Hα and 171 Å, respectively, and numbered thick lines in both rows show that they are especially "conspicuous" ejections. We mainly studied the event which occurred at 04:46 UT on May 2 (event 7 in Figs. 4.1 and 4.2 and Table 4.1), because the ejection was clearly seen both in Hα and in EUV.

4.3   Results and Discussions

4.3.1   Motions of Hα surges

During the observation of DST, which was about 6.5 hr, Hα surges were ejected intermittently from the light bridge of the sunspot umbra in NOAA AR 8971 (see Fig. 4.1). Figure 4.2 shows eight surges which extended to larger than 11,000 km in apparent length. They are the largest among a number of surges observed in this light bridge. In Figure 4.2, the top left image is at H$\alpha - 5.0$ Å, and the others are at H$\alpha - 0.6$ Å. The mean apparent velocity of these surges is about 40 km s^{-1}, the mean apparent maximum length is about 17,000 km, and the mean lifetime is about 10 minutes. These features of the eight surges are listed in Table 4.1. We correct these values for the the projection effect. Assuming that the surges are vertically ejected from the solar surface, we get the velocity of 50 km s^{-1} and the maximum length of 20,000 km. The surges we observed are a few times smaller in velocity and about an order of magnitude smaller in maximum length than those described by Tandberg-Hanssen (1995).

Table 4.1: Apparent velocity and maximum length of large surges

Event	Time (UT)	Apparent velocity (km s^{-1})	Apparent max. length (Mm)
		Hα	
1	00:40	37.1	19.9
2	02:38	32.3	23.2
3	02:50	41.0	15.9
4	03:19	57.3	17.0
5	03:57	44.0	14.2
6	04:27	28.3	14.2
7	04:46	40.4	13.9
8	05:32	. . .	15.6
Mean value	. . .	38.5	16.7
		EUV 171 Å	
7	04:46	41.5	. . .

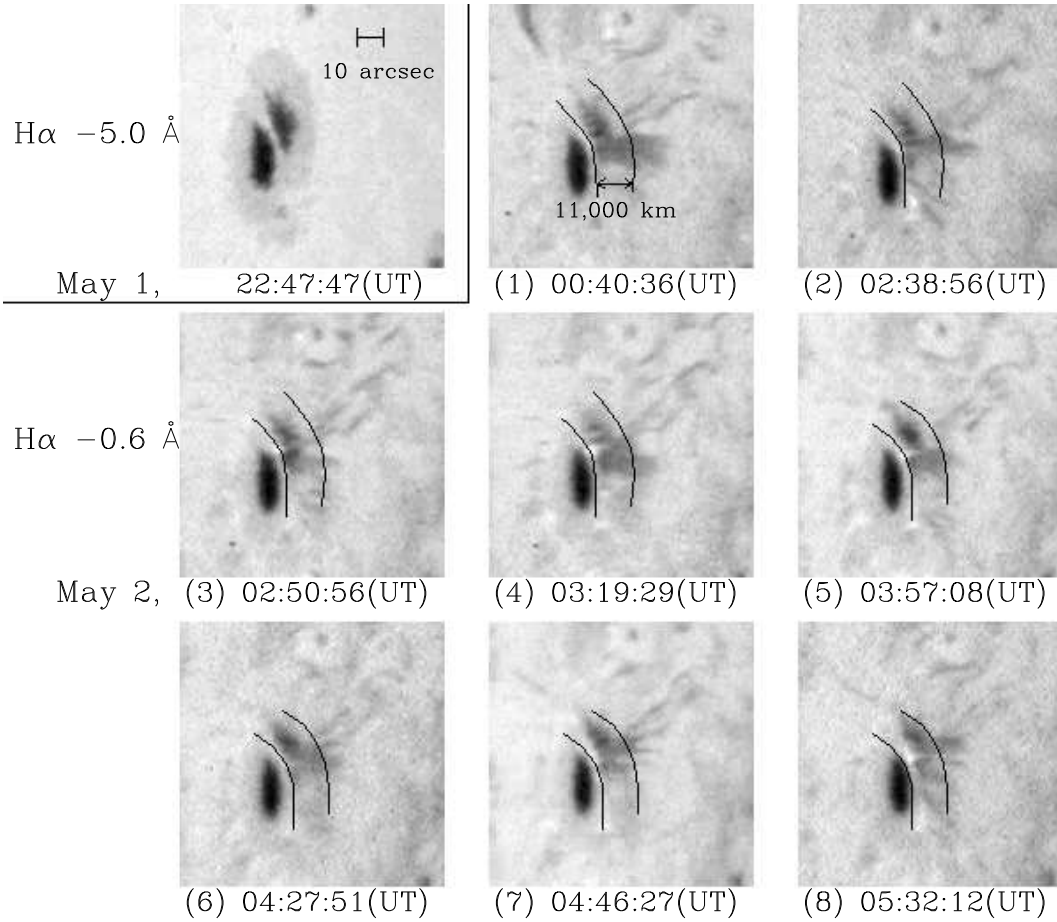Figure 4.2: Eight large Hα surges. Celestial north is up, and west is to the right. The top left image, which clearly shows the light bridge studied in this work, is the image at Hα − 5.0 Å, and the others are at −0.6 Å. The separation of two curved lines, one of which is along the light bridge, is about 11,000 km.

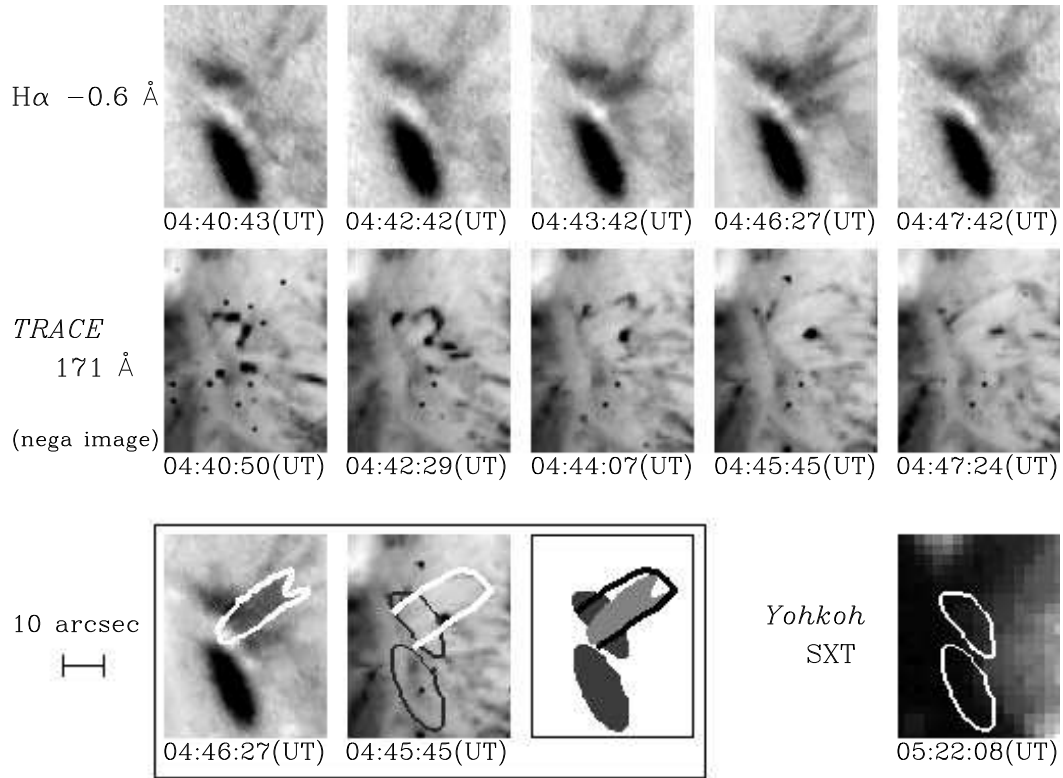Figure 4.3: Temporal evolution of event 7 ejection in DST Hα (*top*), *TRACE* 171 Å (*middle, negative*). Solar north is up, and west is to the right. The bottom right panel is a *Yohkoh*/SXT image, where two white ellipses show the locations of the sunspot umbrae. No bright ejection is seen along the light bridge in the SXT image. The three panels in the bottom left box give the comparison of the appearance and the position of the Hα surges with those of the 171 Å ejections. In the rightmost panel, the umbra, the Hα surge, and *TRACE* 171 Å loop are displayed as dark gray, light gray, and black curved line, respectively. The ejection is seen as a jet in Hα − 0.6 Å, but a loop at 171 Å with *TRACE* .

4.3.2 Comparison with *TRACE* and *Yohkoh*/**SXT** images

We also found ejections from the light bridge in 171 Å images obtained with *TRACE*. These 171 Å ejections have occurred intermittently just as Hα surges. For the event of 04:46 UT (event 7 in Figs. 4.1, 4.2, and Table 4.1), we compared the Hα surge with the 171 Å ejections with respect to their morphological and dynamical characteristics.

Figure 4.3 shows the evolution of the ejection in Hα − 0.6 Å(*top*) and *TRACE* 171 Å (*middle, negative*). The bottom right panel is a *Yohkoh* SXT image overlaid with the contour of the sunspot umbra. The three panels in the bottom left box show the comparison of the appearance and the site of the ejections. The rightmost panel in the box gives the spatial relation among the sunspot umbra, the Hα surge, and *TRACE* 171 Å loop, where they are displayed as dark gray, light gray, and black curved line, respectively. The timing and location of the ejections in *TRACE* 171 Å images are almost the same as those of the surges at Hα − 0.6 Å. Furthermore, the velocity of the 171 Å ejection is about 40 km s^{-1}, and it is nearly equal to that of Hα surge (see Table 4.1). However, the appearance of the ejections in the Hα images and the EUV images are different; that of the Hα surge is like a jet, while that of the 171 Å ejection looks like a reverse U-shaped loop.

The Hα surges seem to be ejected along some open magnetic field lines of about 5,000 km in width, and about 12,000 km in length. On the other hand, the 171 Å ejections (hot plasma) are reverse U-shaped loops that trace the edge of Hα surges (cool plasma; see the bottom middle cartoon in Fig. 4.3). The separation of two foot points of the loop is about 5,000 km, and the loop top is about 12,000 km in hight. The growth of the reverse U-shaped 171 Å loops indicates the existence of some bipolar magnetic polarities in the light bridge of the sunspot umbra. In addition, as will be discussed below with the magnetograms (§4.3.3), the emergence of some new magnetic flux is probably occurring there. We examined soft X-ray images for the same region obtained with *Yohkoh*/SXT, which provide information of the plasma of much higher temperature (more than 3 MK). However, we did not find any SXT ejections according the locations of the Hα surges and EUV ejections in the light bridge. Such differences between the appearance of cool (about 10^4 K) surges in Hα and hot plasma ejections in 171 Å (about 10^6 K) and in soft X-ray (more than 3 MK) images indicate some dynamical and thermal characteristics of plasma ejection in the light bridge of the sunspot umbra. They should be explained by a proper model of the accelerating and heating mechanism.
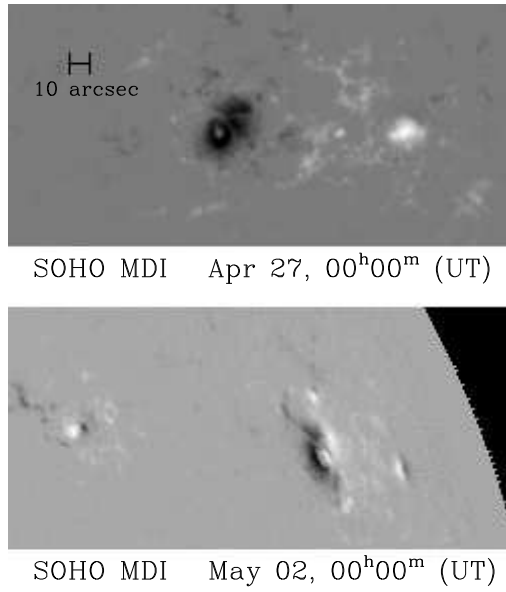
Figure 4.4: Magnetogram of NOAA AR 8971 obtained with *SOHO* MDI on April 27 (*top*) and May 2 (*bottom*). Solar north is up, and west is to the right. The umbrae and the light bridge studied here clearly show a black polarity on April 27. On May 2, however, some fairly white polarity can be seen at the location of the light bridge.

4.3.3 Magnetic Configuration

The continuous surge activity, which was found in the light bridge of the sunspot umbra (§4.3.1), is considered to be evidence of emerging magnetic flux (e.g., Kurokawa & Kawai 1993). The reverse U-shaped loop seen in *TRACE* images (§4.3.2) also suggests the emergence of a bipolar magnetic flux.

Figure 4.4 shows the magnetograms on April 27 (*top*; near the disk center) and on May 2 (*bottom*; near the northwest limb, N20°, W55°) obtained with the Michelson Doppler Interferometer (MDI) on board the *Solar and Heliospheric Observatory* (*SOHO*; Scherrer et al. 1995). The sunspot has negative polarity (*black*). The polarity of the light bridge is also negative, though its field strength is much weaker than the main sunspot umbra (April 27; *top*). On May 2 (*bottom*), positive polarity (*white*) is seen at the location on the light bridge.

Since the sunspot is located close to the solar limb (55°) on May 2, it is difficult to determine whether this opposite polarity is an indication of the newly emerging magnetic flux or whether it appears only due to the projec-

tion effect of the negative polarity field. We cannot exclude the possibility that some negative polarity which is inclined more than about 40° from the normal produces the fake positive polarity. Nevertheless, we suggest that unresolved and small newly emerging magnetic flux plays an essential role in the long-lasting surge activity. To conclude that new bipolar magnetic fluxes really emerge in light bridges and produce such surge activities by magnetic reconnection, we need more precise observations of magnetic fields of light bridges, near the disk center and with higher spatial resolution.

4.4 Summary

We studied dynamical characteristics of Hα surges along a light bridge in a sunspot umbra with DST at Hida Observatory. The surge activities continued intermittently for a long time, at least 6.5 hr. The apparent velocity of the surges was about 50 km s^{-1} on average, and it is typical for that of an Hα surge. We also studied the ejections from the light bridge observed in the EUV coronal line at 171 Å with *TRACE* for the first time. The apparent velocities of 171 Å ejections were almost equal to those of Hα surges. We could not find any ejections from the light bridge in *Yohkoh*/SXT images. This means that the temperature of the plasma ejected from the light bridge is lower than a few megakelvins. We found morphological differences between Hα surges and 171 Å ejections; the 171 Å ejections seem to be loops, while the Hα surges are like jets. Examining the magnetogram obtained with *SOHO* MDI, we suggest that the emergence of new flux occurs in the region, though we cannot exclude the possibility that the opposite polarity is due to a projection effect. We need more precise observations of magnetic fields of light bridges.

Bibliography

Beckers, J. M., and Schröter, E. H., 1969, Solar phys., 10, 384

Bruzek, A., and Durrant, C. J., 1977, Astrophysics and Space Science Library, 69, Illustrated Glossary for Solar and Solar-Terrestrial Physics, (Dordrecht: Reidel)

Handy, B. N., et al., 1999, Solar phys., 187, 229

Kurokawa, H., 1988, VA, 31, 67

Kurokawa, H., & Kawai, G., 1993, in ASP Conf. Ser., 46, The Magnetic and Velocity Fields of Solar Active Regions, ed. H. Zirin, G. Ai, & H. Wang (San Francisco: ASP), 507

Roy, J. R., 1973, Solar phys., 28, 95

Scherrer, P. H., et al., 1995, Solar phys., 162, 129

Schrijver, C. J. et al., 1999, Solar phys., 187, 261

Tandberg-Hanssen, E., 1995, Astrophysics and Space Science Library, 199, The Nature of Solar Prominences, (Dordrecht: Kluwer)

Tsuneta, S., et al., 1991, Solar phys., 136, 37

Yokoyama, T., & Shibata, K., 1995, Nature, 375, 42

Chapter 5

Future Directions

We have examined active phenomena seen on the solar surface, and the relation between such phenomena and the magnetic structure at the active regions.

Solar Flares

We have examined the fine structures at the solar flare (see Chap. 2). The more detailed examinations are difficult because they are restricted with the instrumental limits. However, we will obtain the data with higher quality soon, because of the launches of artificial satellites of the next-generation, e.g., HESSI[1] and Solar-B[2]. We hope that those new instruments will bring us various foundings, and a lot of researches will be developed. Then we now have to study how to derive the most useful informations.

To examine the non-thermal particles with Hα and EUV images, we also have to study the response of the lower solar atmosphere, the transition region and the chromosphere to the precipitation of non-thermal particles, and we have to derive the precise informations of the non-thermal particles from a lot of mechanisms of brightenings.

Solar Jets

The studies of solar jets are important, since they can be prototypes of various astrophysical jets, such as AGN[3] jets that belong to the maximum class in the scale. We have found the solar jets in the EUV wavelengths, and examined them for the first time. They have shown various

---

[1]High Energy Solar Spectroscopic Imager

[2]a Japanese Institute of Space and Astronautical Science (ISAS) mission proposed as a follow-on to the highly successful Japan/US/UK *Yohkoh* (Solar-A)

[3]active galactic nuclei

features, some are common and some are much different compared with
Hα surges and X-ray jets. We now have to try to unify these phenom-
ena, solar jets, to understand the 3-D structure of plasma ejections by
multiwavelength observations. This will enable us to understand more
about astrophysical phenomena.

Prediction of Active Phenomena

We have examined the relation between the active phenomena and the
environmental and global magnetic structure. If we know the process
of formation such structure, we will be able to predict the occurrence
of the events. The studies about the magnetic structures and their for-
mations will bring us the basic understandings of the solar-terrestrial
environment, which contributes to the new field, space whether re-
search.

Acknowledgements